Characterization of two isoforms of a novel ammonia transporter, LpHIAT1α and LpHIAT1β, in the American horseshoe crab *Limulus polyphemus*

by

Maria Eckhardt

A Thesis submitted to the Faculty of Graduate Studies of
The University of Manitoba
in partial fulfillment of the requirements of the degree of

MASTER OF SCIENCE

Department of Biological Sciences
University of Manitoba
Winnipeg

Abstract

The American horseshoe crab, *Limulus polyphemus*, excretes nitrogenous waste in the form of highly toxic ammonia across their book gills. The mechanism of this branchial excretion is yet unknown. In another marine arthropod, the green crab *Carcinus maenas*, a novel ammonia transporter has been discovered and shown to be expressed in the gills. In the current study, two isoforms of this transporter, LpHIAT1α and LpHIAT1β, have been identified in *L. polyphemus*. Both isoforms have 12 predicted transmembrane regions and share 82.7% of amino acid identity to each other. Significantly higher mRNA expression levels of LpHIAT1α were observed in the peripheral mitochondria-poor region of the gill (PMPA), central mitochondria-rich region of the gill (CMRA), and in the brain compared to the LpHIAT1β isoform. Heterologous expression of LpHIAT1α and LpHIAT1β in *Xenopus laevis* oocytes resulted in a significantly lower uptake of the radiolabeled ammonia analogue ^{3}H-methylamine compared to water-injected control oocytes, suggesting an excretory function of this transporter. Exposure to elevated environmental ammonia (HEA, 1 mmol l^{-1}) caused an increase in mRNA expression of LpHIAT1β in the ion-conductive ventral gill half. The high mRNA expression of both isoforms in the brain, and the LpHIAT1α- and LpHIAT1β-mediated methylamine excretion suggest that these highly conserved ammonia transporters have an imperative protective function in cellular ammonia detoxification.

Acknowledgements

I would first like to thank my thesis advisor Dr. Dirk Weihrauch, who has helped shape me into a researcher with his invaluable knowledge, patience, and support. The welcoming yellow "Minion" door to Dirk's office was always open, whether I needed advice on an experiment or writing, or just for a friendly chat. I am grateful to have had such a dedicated mentor to guide me through my Master's experience, who consistently allowed me to explore my own research ideas and steered me in the right direction whenever I needed it. I would also like to thank my committee members, Dr. Kenneth Jeffries and Dr. Gary Anderson, for their guidance and constructive feedback over the last two-and-a-half years.

The present and past members of the "Crab Lab" are what truly made this experience worthwhile- thank you Alex, Garett, Sandra, Aaron, Mikyla, and Nathalie, it was beyond enjoyable to share my time in the lab with you all. Dr. Alex Quijada-Rodriguez enthusiastically helped me develop my entire skill set related to molecular techniques and statistical analysis, editing the manuscript based on this thesis, and moral support during times of despair – thank you, Alex, for being such a wonderful mentor. Dr. Garett Allen – thank you for always providing prompt and elaborate feedback on all things physiology related. Mikyla – I cannot overestimate your help and moral support over the last three years, and am so grateful to have shared this experience with you and gained a lifelong friend in the process.

I would also to like extend my sincere thanks to fellow under-/graduate students: Dr. Haonan Zhouyao and Ruotong Liu from the Eck lab in Human Nutritional Sciences for all their help, advice, and guidance in all things oocyte-related, and Asis Osahan from the Campbell lab for his advice on gene synthesis technology that helped me finally clone the LpHIAT1β isoform.

I would also like to acknowledge the staff at the Animal Holding Facility for caring for my research animals and helping with the frog handling that made a large portion of the experiments in this thesis possible.

Lastly and most importantly, I would like to express my deepest appreciation to my husband Dimitri, my parents, and the rest of my family. Starting my Master's journey at the beginning of a global pandemic brought on a tidal wave of uncertainty, and your unwavering love and support served as a grounding rock at all times.

This study was funded by the NSERC Discovery Grant, Graduate Enhancement of Tri-Agency Stipends, and the Science Enhancement of Grant Stipends.

Thesis Contributions

A condensed form of this thesis is currently in the process of submission to the Journal of Comparative Biochemistry and Physiology- Part B: Molecular & Integrative Physiology.

The RNA samples of horseshoe crab tissues (brain, coxal gland, gill regions) and of the gill regions exposed to short-term (7-9 days) HEA and hypercapnia were used from a previous study conducted by Stephanie Hans (Hans et al., 2018). Dr. Michael Romero kindly provided us with the PGemHE® expression vector used in this study. Dr. Alex R. Quijada-Rodriguez assisted in the functional radioisotope experiments and in editing the manuscript based on this thesis. Dr. Dirk Weihrauch assisted in editing the manuscript, study design, and provided financial assistance. All experiments and data were conducted, collected, analyzed, and presented by Maria Eckhardt.

Table of Content

List of Tables

List of Figures

List of Abbreviations

ANOVA, Analysis of Variance

CA-2, Cytoplasmic carbonic anhydrase

cDNA, Complementary deoxyribonucleic acid

CMRA, central mitochondria-rich area of the horseshoe crab gill

fg, Femtogram

HAT, Vacuolar-type H^+-ATPase

HCN, Hyperpolarization-activated cyclic nucleotide-gated K+ channel

HEA, High environmental ammonia

HIAT1, Hippocampus-abundant transporter 1

Mfsd, Major facilitator superfamily domain

ng, Nanogram

NHE, Na^+/H^+-exchanger

NKA, Na^+/K^+-ATPase

ORF, Open reading frame of gene

Pa, Pascal

pCO_2, Partial pressure of CO_2

PCR, Polymerase chain reaction

pg, picogram

pKa, Dissociation constant

PMPA, peripheral mitochondria-poor area of the gill

qPCR, Quantitative polymerase chain reaction

Rh, Rhesus protein

RNA, Ribonucleic acid

SEM, Standard error of the mean

T_{Amm}, Total ammonia (NH_3 and NH_4^+)

TMD, Transmembrane domain

1.0 Introduction

1.1 *Ammonia*

Nitrogenous waste is inherently produced and excreted by all animals, most commonly in the form of ammonia, urea, or uric acid. The majority of nitrogenous waste generated by animals is derived from the catabolism of proteins and amino acids, where the deamination of amino acids such as glutamine, glutamate, serine, and asparagine by their respective deaminases releases ammonia molecules (Brody, 1999). A small portion of ammonia is produced as a result of the degradation of nucleic acids, specifically the deamination of adenosine monophosphate (AMP) *via* the purine nucleotide cycle, or purine and pyrimidine nucleotide bases *via* the uricolytic pathway (Cooper and Plum, 1987).

Strategies of nitrogen excretion vary widely across the animal kingdom, with most aquatic invertebrates and bony fishes considered ammonotelic (Larsen et al., 2014; Weihrauch and Allen, 2018; Wright, 1995), meaning they predominantly excrete their nitrogenous waste in the form of ammonia. In comparison to other nitrogenous waste products, such as urea or uric acid, ammonia is more toxic but highly water soluble, making it an energetically cheap excretion strategy for aquatic animals as it does not require additional energy to be converted to less toxic forms and the copious water availability provides a diffusion gradient for continuous excretion.

As a weak base, ammonia exists in forms of gaseous, membrane permeable NH_3 or as ionised NH_4^+ (ammonium), where NH_3 can reversibly react with H^+ to form NH_4^+ (Eqn. 1). In this study, NH_3 refers to gaseous ammonia, NH_4^+ to the ammonium ion, and ammonia to the combination of both. Within a solution, the proportions of both forms are determined by pH due to an equilibrium constant (pK_a) of 9.2-9.8, which can vary with temperature, ionic concentration, and pressure (Cameron and Heisler, 1983). Therefore, at a typical physiological pH of 7.2-7.8, most

of the ammonia exists in the ionised NH_4^+ state (Larsen et al., 2014). The relationship between the two forms is as follows:

$$NH_3 + H_2O \leftrightarrow NH_4^+ + OH^- \quad \text{(Eqn. 1)}$$

Given this relationship, ammonia may serve a role in acid-base homeostasis by means of NH_4^+-mediated H^+ excretion, as suggested for the cephalopod *Octopus vulgaris*, where higher rates of proton removal across perfused gills following an induced acidosis was accompanied by a 16-fold higher branchial NH_4^+ excretion rate (Hu et al., 2017). Similarly, in the American lobster (*Homarus americanus*), a 2-week acclimation to climate change conditions predicted for the year 2300 (ca. 948 Pa pCO_2, pH 7.10, 20°C) resulted in a >100% increase in hemolymph ammonia concentration and a 43% increase in ammonia excretion rate (Klymasz-Swartz et al. 2019). Comparatively, acute exposure of American horseshoe crabs (*Limulus polyphemus*) to acidic seawater (pH 6.1) resulted in increased ammonia excretion rates, whereas animals exposed to alkaline seawater (pH 9.0) decreased their ammonia excretion (Hans, 2016). Under alkaline conditions, reducing the ammonia excretion rate should allow the animal to hold on to acid equivalents, whereas acidic conditions might impose an inward H^+-flux into the hemolymph space across the highly ion-permeable ventral epithelium of the gill (Hans et al., 2018), which could be counteracted by an increased ammonia excretion rate to reduce the hemolymph acid load.

1.1.1 Toxicity of ammonia

Excess ammonia may exhibit toxic effects by acting as a H^+-gradient uncoupler within the mitochondria, where NH_3 is generated from the deamination of glutamate (Brody, 1999). Here, NH_3 follows an outward-directed P_{NH_3} gradient into the intermembrane space, where it binds H^+

to form NH_4^+, and thereby disrupting transmembrane H^+ gradients and H^+-dependent processes such as oxidative phosphorylation (O'Donnell, 1997). Ammonia can also impair the optimal functioning of lysosomal proteases in lysozymes by disrupting their intracellular pH if trapped in the form of NH_4^+ inside these acidic vesicles (Larsen et al., 2014).

Ammonia acts as a strong neurotoxin in mammals, causing cytotoxic cerebral edema, changes in blood-brain barrier permeability and neurotransmission, and eventual cell death (Braissant et al., 2013; Butterworth, 2002). In the brain, ammonia (NH_3) has been suggested to inhibit the Na^+-dependent re-uptake of glutamate into astrocytes, which causes an increased activation of *N*-methyl-D-aspartate (NMDA) receptors by excess glutamate in the post-synaptic neuron, and thereby an increased Ca^{2+}-influx and eventual cell death (Marcaida et al., 1992). The increased glutamine synthesis in astrocytes due to lack of glutamate re-uptake in turn causes osmotic swelling and brain edema, followed by cell death (Norenberg et al., 1997). Ionised NH_4^+ can also enter K^+-utilizing transporters, due to the similarity in ionic radius between both ions (Choe et al., 2000), possibly affecting the membrane potential and neuronal excitability.

In aquatic arthropods, hyperammonemia due to high environmental ammonia exposure (HEA) has been shown to disrupt ion regulation in the lobster *Homarus americanus* (Young-Lai et al., 1991), ion permeability in the green shore crab *Carcinus maenas* (Spaargaren, 1990), energy metabolism in the water flea *Daphnia magna* (Nash et al., 2022), and a growth reduction in juvenile tiger shrimp *Penaeus monodon* (Chen and Chen, 1992). Ammonia toxicity increases as pH in seawater decreases to ca. pH 7.0 (Eddy, 2005), furthermore enhancing its toxic effects on marine life with acidifying ocean conditions as projected for the year 2300 (Caldeira and Wickett, 2005).

1.1.2 Transport proteins involved in ammonia transport/excretion

To avoid detrimental effects, ammonia must be converted into less toxic forms such as urea or uric acid, or directly excreted *via* internal or external excretory organs. As mentioned earlier, aquatic invertebrates are generally ammonotelic and predominantly excrete ammonia as their nitrogenous waste product (Larsen et al., 2014; Weihrauch and Allen, 2018b; Wright, 1995). Due to the abundant water availability that large bodies of water provide, it was long believed that ammonia excretion across the gills of aquatic invertebrates was a purely passive process, following an outward-directed NH_3 partial pressure gradient (Larsen et al., 2014). However, active ammonia excretion has been reported in the gills of some crustaceans, such as the green shore crab (*C. maenas*) and the Chinese mitten crab (*Eriocheir sinensis*), the marine edible crab (*Cancer pagurus*) (Weihrauch et al., 1999), and the Dungeness crab (*Metacarcinus magister)* (Martin et al., 2011a). At the time of writing this thesis, only one previous study investigating gene expression of common transporters involved in ammonia excretion had been conducted in marine chelicerates (Hans et al., 2018) and the mechanism of excretion is not yet understood.

Previous investigations on ammonia excretory mechanisms in other invertebrates have suggested the involvement of several key transporters, such as the Na^+/K^+-ATPase (NKA), V-type H^+-ATPase (HAT), Rhesus (Rh) proteins, and a hyperpolarization-activated cyclic nucleotide-gated K^+ channel (HCN) (Fehsenfeld and Weihrauch, 2016; Fehsenfeld and Wood, 2020; Hans et al., 2018).

In addition to following a passive paracellular route, the ammonium ion (NH_4^+) shares a similar ionic radius to a K^+ ion and can enter K^+-channels and K^+-utilizing transporters such as the NKA as a substrate (Choe et al., 2000; Hans et al., 2018; Masui et al., 2003; Weihrauch et al.,

1998). It has been suggested that the V-type H^+-ATPase (HAT) is involved in creating an outward-directed transmembrane NH_3 gradient by acidifying the unstirred boundary layer of the apical membrane (Adlimoghaddam et al., 2015; Quijada-Rodriguez et al., 2015; Weihrauch et al., 1998), which allows gaseous NH_3 to simply diffuse across the cell membrane (Martinelle and Häggström, 1993) or *via* the dual NH_3/CO_2 gas channel Rhesus (Rh) proteins (Adlimoghaddam et al., 2015; Hans et al., 2018; Hu et al., 2017; Marini et al., 2000; Martin et al., 2011a; Nawata et al., 2010; Quijada-Rodriguez et al., 2015; Thiel et al., 2017). Additionally, the facilitation of ammonia excretion by a carbonic anhydrase (CA) has been suggested (Henry et al., 1997). Salinity studies in brachyuran crabs identified a cytoplasmic and a membrane-bound CA (Henry et al., 2003; Serrano and Henry, 2008), with precise roles in ammonia excretion not yet fully understood. Protons (H^+) produced as a result of the reversible hydration of CO_2 catalyzed by a membrane-bound CA could serve to protonate any excreted NH_3, and thereby maintain the P_{NH3} gradient similarly to a V-type H^+-ATPase (Henry et al., 1997), whereas H^+ produced by a cytoplasmic CA could be recruited by H^+-transporters involved in ammonia excretion such as the HAT.

More recently, two ammonium transporters (AMT's; part of the methylammonium permease/ammonium transporter (Mep/Amt) family of transporters) have been identified and characterized in the anal papillae and reproductive tracts (AeAMT1) of the mosquito *Aedes aegypti* (Chasiotis et al., 2016; Durant and Donini, 2020, 2018), providing evidence for the first AMT-facilitated ammonia excretion in animals, and a crucial role of AeAMT1 in spermatogenesis and male fertility in *A. aegypti*.

1.2 *Limulus polyphemus*

Commonly known as “living fossils”, the American horseshoe crab (*Limulus polyphemus;* Arthropoda; subphylum Chelicerata; subclass Xiphosura) has remained practically unchanged in morphology for over 150 million years (Avise et al., 1994). Despite their name, horseshoe crabs are phylogenetically more closely related to spiders, mites and ticks (Chelicerata) than to crabs (Crustacea). Horseshoe crabs (*L .polyphemus*) have contributed to the medical field following the discovery of *Limulus* amoebocyte lysate (LAL), a lipopolysaccharide employed for the detection of bacterial endotoxins in biological and commercial fluids since the 1970’s (Elin and Wolff, 1973).

American horseshoe crabs populate estuarine habitats along the Atlantic East Coastline of the Unites States during all of their juvenile life and much of their adult life, as they exhibit an annual migration from deeper marine waters to shallow, fluctuating estuarine areas and spawning beaches during their mating season (Brockmann, 1990), which may impose hypercapnic (elevated ambient pCO_2) conditions on the animals. These ammonotelic chelicerates likely spend a considerable time burrowed in the sediment foraging for food in their natural habitat (Shuster, 2015). Sediments of benthic habitats often present higher-than-ambient ammonia levels (Stoeckel et al., 2011; Weihrauch et al., 1999), likely as a result of the animals’ metabolic waste accumulation and the low water circulation while burrowed (McGaw, 2005). To successfully navigate these conditions and to avoid toxic systemic ammonia loads, *L. polyphemus* require an efficient ammonia excretion mechanism that is not yet fully understood.

1.2.1 Book gills and current understanding of ammonia excretion in L. polyphemus

Results of one previous study investigating ammonia excretion and acid-base regulation in the American horseshoe crab (*Limulus polyphemus)* provide evidence that the book gills of *L. polyphemus* play a role in ammonia excretion (Hans et al., 2018). The gills of *L. polyphemus* are comprised of 5 pairs of book gills (Fig. 1), with each book gill made of around 150 individual lamellae that are ventilated during swimming motion. These gills exhibit physiological (Hans et al., 2018) and ultrastructural differences (Henry et al. 1996, Fig. 2) with a highly ion-conductive ventral half-lamella and an ion-tight dorsal half-lamella, as well as a central mitochondria-rich area (CMRA) and a peripheral mitochondria-poor area (PMPA). The ion-conductive ventral half-lamella can be characterized by the presence of the CMRA as depicted in Figure 3.

On the molecular level, the ventral half-lamella can be differentiated by a higher relative mRNA expression of LpRh-1, CA-2 and HCN compared to the dorsal-half lamella, whereas the dorsal half-lamella exhibited a higher transcript abundance of LpRh-2 (Hans et al., 2018).

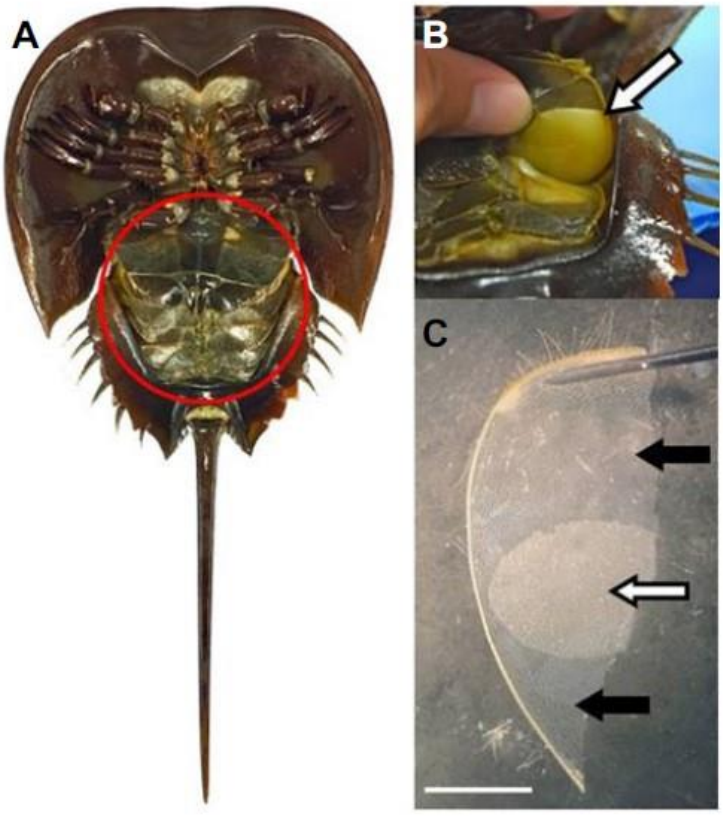

Figure 1. Gills of the American horseshoe crab (*Limulus polyphemus*). (**A**) Ventral side of an adult horseshoe crab, with book gills circled in red. (**B**) A single book gill (white arrow) comprised of hundreds of individual lamellae. (**C**) An individual gill lamella, comprised of a central mitochondria-rich area (CMRA, white arrow) and a peripheral mitochondria-poor area (PMPA, black arrows). Each lamella is comprised of two single-celled epithelia (dorsal and ventral side). Scale bar depicts 0.5 cm. Images taken by Stephanie Hans, and published in Hans et al. 2018.

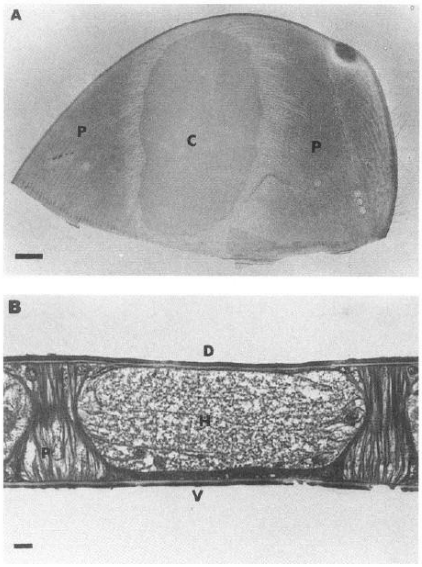

Figure 2. Ultrastructural composition of an American horseshoe crab gill (*L. polyphemus*). (**A**) Whole mount of an individual gill lamella depicting central (C) and peripheral (P) regions. Scale bar = 2 mm. (**B**) Longitudinal section through a lamellar central region depicting a thinner, ion-tight dorsal (D) and thicker, ion-conductive ventral (V) epithelial layer. The epithelial layers are separated by hemolymph space (H) and supported by pillar cells (P). Scale bar = 10 µM. Images published in Henry et al 1996.

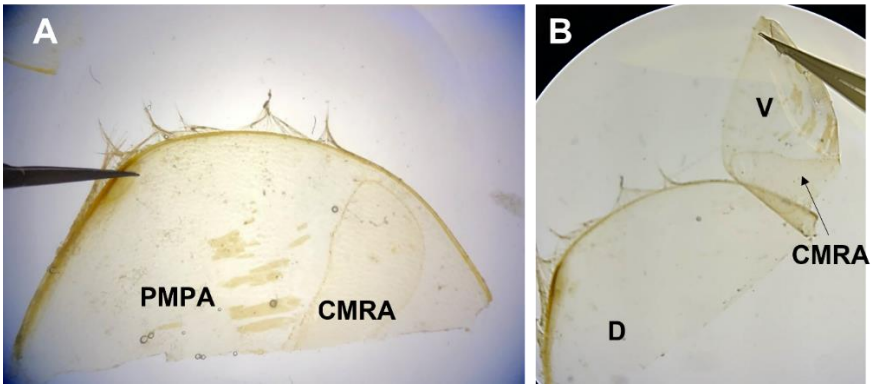

Figure 3. Gill lamella isolated from *Limulus polyphemus* depicting (**A**) the central mitochondria-rich area (CMRA) and a peripheral mitochondria-poor area (PMPA). (**B**) Split gill lamella of *L. polyphemus* depicting the dorsal (D) epithelial layer and the ventral (V) epithelial layer characterized by the presence of the CMRA patch. © Maria Eckhardt 2022.

In flux-experiments, where each epithelial layer of the gill lamella was mounted in an Ussing chamber to observe the lamellar transepithelial conductance (G_{TE}) and transepithelial ammonia fluxes, the dorsal lamella exhibited an almost negligible conductance (G_{TE} 0.2 ± 0.04 mS cm^{-2}) compared to the highly conductive ventral-half lamella (G_{TE} 145.4 ± 33.95 mS cm^{-2}) (Hans et al., 2018). When *in-vivo* ammonia conditions were applied (ca. 300µmol l^{-1} ammonia basolateral side, 0 µmol l^{-1} ammonia apical side), an ammonia efflux across the ventral epithelium was detected at a rate of 220.28 ± 63.89 nmol cm^{-2} h^{-1}, whereas no transepithelial ammonia transport was detected across the dorsal half-lamella (Hans et al., 2018).

When whole animals were acclimated to high environmental ammonia conditions (HEA; ca. 1 mmol l^{-1} NH_4Cl) for 7-9 days, ammonia influx occurred *via* the ion-permeable ventral epithelium of the gill but was excreted against its gradients *via* the dorsal epithelium. The dorsal half-lamella was able to maintain near-control basolateral ammonia levels against a ca. 3-fold inward gradient, suggesting an active ammonia excretion across the dorsal-half epithelium under HEA conditions (Hans et al., 2018).

Following HEA exposure, quantitative PCR (qPCR) gene expression analysis revealed a significantly higher mRNA transcript abundance of V-type H^+-ATPase subunit B (HAT), cytoplasmic carbonic anhydrase-2 (CA-2), and hyperpolarization-activated cyclic nucleotide-gated K^+ channel (HCN) in the ventral-half lamella, and roughly 2-fold higher CA-2 and 3-fold higher Rhesus protein-1 (LpRh-1) expression levels in the dorsal-half lamella; suggesting an involvement of these transporters in the branchial ammonia excretion in *L. polyphemus* (Hans et al., 2018)

The mean hemolymph ammonia concentration of horseshoe crabs under control conditions was reported to be 320.8 ± 36.9 μmol l^{-1}. The hemolymph ammonia concentration remained largely unchanged (334.0 ± 28.3 μmol l^{-1}) after 7-9 days of HEA exposure, and significantly decreased to 183.8 ± 19.69 μmol l^{-1} under high CO_2 conditions (Hans et al., 2018).

In addition to the gills, the coxal gland of *L. polyphemus* is another site potentially involved in ammonia excretion. The coxal gland, an organ homologous to the crustacean antennal gland (Henry et al., 1996), has been shown to produce a hypo-osmotic and hypo-ionic urine (compared to the hemolymph) under low salinity conditions (Mangum et al., 1976; Towle et al., 1982), and in conjunction with its' high NKA activity (Towle et al., 1982), has been suggested to contribute to ion regulation and potentially ammonia excretion under HEA stress (Hans et al., 2018).

1.3 *HIAT1 transporter (hippocampus abundant transcript 1)*

In addition to the above-mentioned transport proteins in section 1.1.2, a transporter of the major facilitator superfamily, HIAT1 (hippocampus-abundant transcript 1, renamed as Mfsd14a in mammals), has recently been identified as a highly conserved, novel ammonia transporter in decapod crabs and teleosts (Fehsenfeld et al., personal communication; Zhouyao et al., under review).

HIAT1 was first discovered in the hippocampus of mice, where it was initially believed to be a novel glucose transporter solely based on the presence of the sugar transporter-specific D-R/K-X-G-R-R/K motif (Matsuo et al., 1997). This assumption, however, has recently been disproven when functional expression of the HIAT1 protein of the green shore crab (*C. maenas*, CmHIAT1) and humans (*Homo sapiens*, MFSD14A) did not promote glucose transport (Fehsenfeld et al., personal communication; Zhouyao et al., 2022).

In mammals, two isoforms of HIAT1 have been reported, namely MFSD14A (HIAT1) and MFSD14B (HIAT1L), both of which were found to be intracellular neuronal membrane-bound proteins (Lekholm et al., 2017). The MFSD14A gene has been found to play a role in spermatogenesis, with sterility reported in mutant HIAT1/ MFSD14A mice as a result of round-headed sperm production similar to globozoospermia observed in humans (Doran et al., 2016). Additionally, a role of MFSD14A in energy metabolism has been suggested after amino acid starvation resulted in a down-regulation of the HIAT1/ MFSD14A gene in the hypothalamus of mice (Lekholm et al., 2017). As an integral membrane protein, HIAT1 exhibits 12 transmembrane domains and is highly conserved among the animal kingdom (ca. 80 % amino acid homology between mammals and crustaceans) and even present in plants and fungi (Fehsenfeld et al., personal communication; Lekholm et al., 2017; Zhouyao et al., under review).

In invertebrates, the HIAT1 transporter was first associated with acid-base balance in the green crab *C. maenas*, when a microarray study discovered a significant down-regulation of this orphan transporter in response to hypercapnia (Fehsenfeld et al., 2011). A follow-up study in *C. maenas* identified a ubiquitous mRNA expression pattern of CmHIAT1, with the highest transcript abundance observed in the osmoregulatory posterior gills and ganglia (Fehsenfeld et al., personal communication). Furthermore, an up-regulation in the abundance of CmHIAT1 mRNA was discovered in the osmoregulatory active posterior gills of the green shore crab after acute (6-24 h) HEA exposure (Fehsenfeld et al., personal communication).

Contrary to the green shore crab, where only one HIAT1 protein is expressed, three paralogues of the HIAT1 transporter (DrHiat1a, DrHiat1b, DrHiat1-like) were identified in zebrafish (*Danio rerio*), where the DrHiat1a and DrHiat1b transporter were shown to mediate uptake of methylamine (an ammonia analogue) in *X. laevis* oocytes. This methylamine uptake

was competitively inhibited after the addition of NH_4Cl, suggesting a DrHiat1b substrate preference for ammonia (Zhouyao et al., under review). Both paralogues, DrHiat1a and DrHiat1b, presented maternal gene expression, with the transcription onset during the maternal-to-zygotic transition stage, and were mainly localized to the head region of *D. rerio* larvae at 24-hours post-fertilization. Expression of both paralogues extended to tissues such as the brain, heart, gills, digestive system, pectoral fins and cranial and lateral line ganglia at 2-4 days post-fertilization (Zhouyao et al., under review). Knockdown of DrHiat1b resulted in an 85 % lower ammonia excretion rate in the pharyngeal region of *D. rerio* larvae, indicating a crucial ammonia excretion role of DrHiat1b in this immature gill region.

1.4 *Objectives and Hypotheses*

The experiments of this thesis aim to characterize and further our understanding of the role of the HIAT1 transporter in arthropods employing the marine chelicerate American horseshoe crab, *L. polyphemus*, as a model.

Considering recent studies of HIAT1 in fish and crustaceans (*D. rerio* and *C. maenas*), along with the transporter's high conservation in the animal kingdom, I hypothesized that:

1. The American horseshoe crab (*Limulus polyphemus*) also expresses the HIAT1 transporter, similar to other marine invertebrates.

2. The HIAT1 transporter is highly expressed in the ammonia-excreting gills of *L. polyphemus.*

3. The *L. polyphemus* HIAT1 transporter mediates ammonia transport.

4. Expression of the *L. polyphemus* HIAT1 transporter is affected by high environmental ammonia and/or elevated environmental pCO_2 conditions.

To accomplish this, the transcriptome of *L. polyphemus* on the GenBank® genetic sequence database (https://www.ncbi.nlm.nih.gov/genbank/) was mined to identify *L. polyphemus*-specific HIAT1 isoforms, followed by sequence-based genetic structure analysis. Furthermore, qPCR analysis will be used to determine mRNA expression levels of HIAT1 in ammonia-sensitive tissues (brain) or tissue potentially involved in ammonia excretion (gills and coxal gland). Responses in HIAT1 transcript abundance within the branchial regions upon acute and short-term environmental ammonia conditions and elevated environmental pCO_2 conditions will be

assessed by qPCR to determine the contribution of HIAT1 in this species' physiological response and fitness. Lastly, functional expression studies employing heterologous expression of *Limulus* HIAT1 in *Xenopus laevis* oocytes will be conducted to evaluate the ammonia transport capabilities of this novel transporter.

2.0 Materials and Methods

2.1 *Sequence-based genetic structure analysis*

The translated HIAT protein sequences for LpHIAT1α (GenBank accession no. XP_013778555.1, 509 amino acids) and LpHIAT1β (GenBank accession no. XM_013929932.2, 494 amino acids) were used as a template to identify the HIAT1 gene in other species using the Basic Local Alignment Search Tool (BLAST) with the Blastp option (NCBI; https://blast.ncbi.nlm.nih.gov/Blast.cgi). Amino acid sequences from 32 species were aligned using the Constraint-based Multiple Alignment Tool (COBALT, NCBI; https://www.ncbi.nlm.nih.gov/tools/cobalt/cobalt.cgi) with the default settings, and the alignment was downloaded in a fasta-plus-gaps format. The Molecular Evolutionary Genetics Analysis program (MEGA X; Jones D.T., Taylor W.R., 1992) was used to generate an evolutionary history by using the Maximum Likelihood method and JTT matrix-based model (Kumar et al., 2018). Initial trees for the heuristic search were obtained automatically by applying Neighbor-Join and BioNJ algorithms to a matrix of pairwise distances estimated using the JTT model, and then selecting the topology with a superior log likelihood value. The tree was drawn to scale, and branch lengths were measured in the number of substitutions per site. The percentage of trees in which the associated taxa clustered together is portrayed next literto the branches. A discrete Gamma distribution was used to model evolutionary rate differences among sites (5 categories

(+G, parameter = 0.6173)). All positions with less than 95 % site coverage were eliminated (i.e., fewer than 5 % alignment gaps) and missing data and ambiguous bases were allowed at any position (partial deletion option). A replicate number of 500 was used for bootstrapping.

Transmembrane models of the LpHIAT1α and LpHIAT1β gene open-reading frames (ORFs) were generated with Protter (Omasits et al., 2014) using the default settings, and potential phosphorylation sites were generated using Scansite 4.0 (Obenauer et al., 2003).

2.2 *Animal care and experimental design*

American horseshoe crabs (*Limulus polyphemus*, carapace width = 15-17 cm; body mass = 410-601 g) were imported from the Marine Biological Laboratory (Woods Hole, MA, USA) to the Animal Holding Facility at the University of Manitoba (Winnipeg, MB, Canada). A maximum of 5 animals were housed at 22°C in a 750-litre tank with aerated and filtered artificial seawater (salinity = 32-33 ppt., pH 8.1; Fritz Reef Pro Mix, Texas, USA) supplied with a live sand bed to allow complete burrowing (CaribSea Inc. Ocean Direct™, FL, USA). Animals were fed a diet of 1 raw mussel or scallop per animal once weekly, with a partial water change performed the day after feeding.

Acute high environmental ammonia (HEA) experiments were set up in a paired fashion, with each animal undergoing a 24-hour control period in the respective experimental environment, followed by a 1-hour recovery period after tissue sampling to account for handling stress, and a 24-hour period in HEA treatment (1 mmol l^{-1} NH_4Cl). A concentration of 1 mmol l^{-1} NH_4Cl was chosen for the HEA treatment under the consideration that past studies on *L. polyphemus* indicate this to be a non-lethal dose (Hans et al., 2018). Horseshoe crabs were fasted for 2 days prior to experiments. During the experiment, horseshoe crabs were maintained individually in 40

litres of gently aerated seawater (salinity = 31-32 ppt.) at room temperature and placed into a pre-equilibrated HEA tank containing ca. 1 mmol l^{-1} NH_4Cl following their control period. Tank water and hemolymph samples of 300 µl were taken at 0, 2, 6, and 24 h, and gill tissue samples were taken at 24 h after the control and HEA treatment. Gill tissue samples consisted of 6 gill lamellae, and each gill lamella was split into its respective dorsal and ventral halves following the procedure outlined in Hans et al. (2018). Tissue samples were then manually homogenized in glass homogenizers with 300 µl of 1x DNA/RNA Protection Reagent (Monarch® Total RNA Miniprep Kit, New England Biolabs, MA, USA) and stored at -80°C until future RNA extraction (see *RNA extraction, cDNA synthesis and quantitative real-time PCR (qPCR)*). Hemolymph was collected from the interdigitating membranes of the legs using a 1 ml syringe and 21-gauge needle. Samples were immediately centrifuged at 5,000 *g* and supernatant (serum) was immediately frozen at -20°C for future ammonia analysis (see *Seawater and hemolymph ammonia analysis*). Tank water samples at each time point were collected and frozen at -20°C for future ammonia analysis.

A previously conducted experiment of horseshoe crabs exposed to short-term (7-9 days) acclimation periods to HEA and elevated pCO_2 (300 Pa) provided the RNA samples for an additional experimental set used in this study, with the methods detailed in Hans et al. (2018).

2.3 *Seawater and hemolymph ammonia analysis*

Horseshoe crab hemolymph samples were deproteinized immediately prior to the spectrophotometric analysis of ammonia content. Previously frozen serum samples (80 µl) were mixed with 80 µl of ice-cold 6% perchloric acid (PCA) and allowed to deproteinize on ice for 10 minutes. Samples were centrifuged at 4°C (5 minutes at 21,000 *g*) and the supernatant was

neutralized with 3 mol l^{-1} KOH. Neutralized samples were centrifuged at 4°C (5 minutes at 21,000 *g*) and the supernatant was used for ammonia analysis. Hemolymph samples from horseshoe crabs acclimated to control conditions were diluted at a 1:5 ratio, whereas hemolymph samples from animals acclimated to HEA were diluted at a 1:10 ratio. Tank saltwater samples from HEA treatment were diluted at a 1:20 ratio. Ammonia standards (0, 5, 10, 20, 40, 60, 80, 100 µmol l^{-1}) were prepared in saltwater as a reference for tank water samples, whereas standards prepared in deproteinized artificial horseshoe crab Ringers solution (in mmol l^{-1}: 260 NaCl, 5 $CaCl_2$, 10.7 $MgCl_2$, 12.1 KCl, 4.4 $NaHCO_3$, 14.1 $MgSO_4$, 0.627 Glucose, pH 7.6) were used as a reference for hemolymph samples.

A salicylate-hypochlorite assay based on Verdouw et al. (1978) was utilized to determine the amount of ammonia in seawater and horseshoe crab hemolymph samples. Briefly, experiments were carried out in 96-well polystyrene microplates in triplicate (Corning™, Fisher Scientific, Ottawa, ON, Canada) and each reaction was prepared in the following order of : 160 µl of sample, 80 µl of a salicylate and catalyst solution and 40 µl of an alkaline hypochlorite solution. The salicylate and catalyst solution consisted of 40 µl sodium salicylate (50% w/v) and 40 µl of sodium nitroprusside (0.02 g / 100 ml water) pre-mixed immediately prior to the experiment. The alkaline hypochlorite solution consisted of a 1:9 ratio of sodium hypochlorite (6%) to alkaline citrate (35 g sodium citrate and 4 g NaOH in 100 ml water). Assays were mixed well by pipetting and incubated in the dark for 60 minutes, followed by spectrophotometric analysis at a wavelength of 650nm (Powerwave, BioTek, Winooski, VT, USA).

2.4 *RNA extraction, cDNA synthesis and quantitative real-time PCR (qPCR)*

The tissue samples used in this study for qPCR analysis consisted of three groups: (1) the central (CMRA) and peripheral (PMPA) gill regions, brain tissue and coxal gland samples, (2) the ventral and dorsal gill epithelial layers from control, short-term HEA (7-9 days), and short-term hypercapnia (7-9 days) acclimated horseshoe crabs, and (3) the ventral and dorsal gill epithelial layers from control and acute HEA acclimation (24-hour). RNA samples from tissues listed in Group 1 and 2 were obtained from a previous study, with the details outline in (Hans et al., 2018).

Gill tissue samples from the acute HEA experiment (Group 3) were dissected and homogenized as described in section 2.2. The RNA was extracted and treated with DNase I using the Monarch® Total RNA Miniprep Kit (New England Biolabs, MA, USA) following the manufacturer's instructions. The RNA concentration and purity were determined on a spectrophotometer (Nanodrop, ND-1000, Thermofisher, Waltham, MA, USA) and RNA integrity was assessed on a 1% agarose gel stained with ethidium bromide. The effectiveness of the DNase I treatment was assessed by employing polymerase chain reaction (PCR) analysis using the elongation-factor-1-alpha (LpEF1α) primer pair (Supplementary Table 1) on the DNase I-treated RNA samples, ensuring that no DNA contamination was present upon gel visualization. Following DNase I treatment, cDNA was synthesized from DNA-free samples with the iScript cDNA synthesis kit (BioRad, Mississauga, ON, Canada). Total RNA quantity used for cDNA synthesis was adjusted based on RNA availability and varied for each tissue group as follows: 0.8 µg RNA for Group 1 tissues, 0.35 µg RNA for Group 2 tissues, and 0.2 µg RNA for Group 3 tissues. Variations in RNA abundance did not affect the analysis of qPCR results, as each tissue group was analyzed separately.

All qPCR experiments were performed with 5 µl 2x Luna® Universal qPCR Master Mix (New England Biolabs, MA, USA), gene-specific forward and reverse primers at a final concentration of 250 nmol (Table 1; Supplementary Table 1) and 2 µl of 1:8 diluted cDNA of each sample in a final reaction volume of 10 µl. A standard curve based on a dilution series of *L. polyphemus* gill cDNA was included in each run. Additionally, a dilution series of known quantities of each respective gene fragment (20 pg - 0.02 fg) was run for absolute quantification purposes for control tissues of Group 3.

Table 1. Primer sequences used in qPCR and cloning of the open-reading frame of HIAT1α and HIAT1β in *Limulus polyphemus*. F= forward primer, R= reverse primer

Application	Name	Sequence (5'-3')	Amplicon size (bp)	Annealing temperature (°C)
qPCR	LpHIAT1α F	TATCATGGGGAGCTAATATTTC	230	53
	LpHIAT1α R	TGCCACAACAGAAAGCAGAC		
	LpHIAT1β F	CCTACGTCCCGGGAGGAAAGCA	184	60
	LpHIAT1β R	CAGCTGAAAATCCCATTACCA		
Cloning/ ORF	LpHIAT1α BamHI F	AAAGGATCCATGCCGAGAAAAATGTCAAG	1548	44
	LpHIAT1α HindIII R	AAAAAGCTTCTATAAAGGTTCTGTGTCTT		
	LpHIAT1β ORF F	ATGCCAAGTAAAATGTCAAA	1485	42
	LpHIAT1β ORF R	CTATAAAGAAACTGAGTCTT		

For relative quantification, the internal standard/housekeeping gene LpEF1α was chosen, as it did not show any significant mRNA expression differences across tissues and treatments (data not shown). The implemented BioRad CFX manager 3.1 software was used to obtain primer efficiency values (> 85%, R^2 >/= 0.99), and the mRNA levels of each target gene were calculated relative to the housekeeping gene (LpEF1α) using the Pfaffl method (Pfaffl, 2004). For absolute

quantification, Ct values obtained from standard curves of known amounts of template were plotted against the respective LOG (template copy number), and the resulting linear regression equation was used to determine copy numbers of each sample using the following equation:

$$\text{Copy number } (\text{ng}^{-1}) = \frac{\text{Amount of DNA template (ng) x } 6.02\times10^{23} \left(\text{molecules mol}^{-1}\right)}{\text{DNA template size (bp)} \times 660 \left(\text{g mol}^{-1}\right) \times 1\times10^{9} \text{ (ng g}^{-1})} \quad \text{(Eqn. 2)}$$

2.5 *Heterologous/ Functional expression of LpHIAT1α and LpHIAT1β in Xenopus laevis oocytes*

2.5.1 Preparation of the open reading frame of LpHIAT1α and LpHIAT1β, plasmids, and capped mRNA

The full open reading frame (ORF) for the LpHIAT1α gene was amplified in a PCR from a *L. polyphemus* gill cDNA template using a Q5® High-Fidelity DNA Polymerase (New England Biolabs (NEB), MA, USA), with primers designed based on the published LpHIAT1α sequence (GenBank accession no. **XP_013778555.1**) including the restriction sites BamHI (T7/5' end; AAAggatccATGCCGAGAAAAATGTCAAG) and HindIII (Sp6/3' end; AAAaagcttCTATAAAGGTTCTGTGTCTT) for directional cloning (Table 1). The full ORF was ligated into the pGEM®-HE expression vector, a modified pGEM®-3Z vector containing the *Xenopus* beta globin 5'- and 3'- UTR sequences, using a 5:1 insert-to-vector ratio and a T4 ligase following the manufacturer's instructions (NEB, MA, USA).

The full ORF for the LpHIAT1β gene was obtained from the published sequence (GenBank accession no. XM_013929932.2), optimized for *Xenopus laevis* expression, and synthesized with the addition of SmaI (5' end) and XbaI (3' end) restriction sites into the GeneArt pMA subcloning plasmid vector using the online GeneArt Gene Synthesis Service by

Thermo Fisher Scientific™. The LpHIAT1β ORF was restriction-digested out of the pMA subcloning vector using the SmaI and XbaI restriction enzymes, and ligated into the pGEM®-HE expression vector using a T4 ligase.

Ligated LpHIAT1α and LpHIAT1β plasmids were transformed and amplified in DH5-α *Escherichia coli* competent cells (Thermo Fisher Scientific™, MA, USA), and plasmid DNA of positive colonies containing the correct gene insert was extracted using the GeneJET Plasmid Miniprep kit following the manufacturer's guidance (Thermo Fisher Scientific™, MA, USA). Sequencing analysis verified the correct gene insert at 100% nucleotide matching to the published reference sequences. The pGEM®-HE plasmid containing the ORFs for LpHIAT1α and LpHIAT1β were linearized with NheI and SphI, respectively. Capped mRNA (cRNA) was transcribed using the HiScribe™ T7 ARCA mRNA Kit (NEB) following the manufacturer's instructions, eluted in 15 µl molecular grade water, and purified using the E.Z.N.A.® MicroElute RNA Clean Up kit (Omega Bio-tek, GA, USA). The cRNA was quantified on a spectrophotometer (Nanodrop, ND-1000, Thermofisher, Waltham, MA, USA) and cRNA integrity was assessed on a denaturing formaldehyde agarose gel in MOPS buffer.

2.5.2 Buffer and oocyte preparation

The standard oocyte ringer (OR2) contained (in mmol l^{-1}) 82.5 NaCl, 2.5 KCl, 1 $CaCl_2$, 1 $MgCl_2$, 1 Na_2HPO_4, 5 HEPES; and was adjusted to pH 7.5 with NaOH. Stage V oocytes were collected from mature female *Xenopus laevis* (VWR, Radnor, PA, USA). The frogs were anesthetized in tricaine methanesulfonate (MS-222), followed by euthanasia *via* decapitation prior to the collection of the ovary. The ovary was placed in Ca^{2+}- free OR2 buffer with collagenase type IV (1 mg ml^{-1}) (Gibco, Waltham, MA, USA) and gently agitated at room

temperature for digestion. The digestion was deemed complete once single oocytes were separated from the ovary membrane, usually after a duration of 3 hours. To terminate the collagenase activity, 1 mmol l^{-1} $CaCl_2$ was added to the buffer solution. Oocytes were manually sorted based on their developmental stage, colour, and shape, and rinsed with standard OR2 solution. For overnight storage of isolated oocytes, OR2 was supplemented with 2.5 mmol l^{-1} sodium pyruvate, 1 mg ml^{-1} penicillin-streptomycin (Gibco, Long Island, NY, USA) and 50 µg ml^{-1} gentamicin and incubated at 18°C. All procedures used were approved by the University of Manitoba Animal Research Ethics Board and are in accordance with the Guidelines of the Canadian Council on Animal Care (Protocol #: F20-021/1).

After the overnight recovery, isolated oocytes were injected with 18.4 ng of cRNA (36.8 nl with 0.5 ng nl^{-1}) or nuclease-free water as control (Sham) using the Nanoject III auto-nanolitre injector (Drummond Scientific, Broomall, PA, USA). Experiments were conducted at room temperature 3 days post-injection.

2.5.3 Microinjections of oocytes: H^3-methylamine transport studies in oocytes expressing LpHIAT1α and LpHIAT1β

Nine oocytes injected with either LpHIAT1α and LpHIAT1β cRNA or nuclease-free water (Sham) were randomly divided into groups of 3 oocytes and incubated at room temperature in 1.5 ml microcentrifuge tubes containing 200 µl of standard OR2 solution (pH 7.5), radiolabelled H^3-methylamine hydrochloride (1 µCi ml^{-1}; Moravek Inc., Brea, CA, USA), and either 1 mmol l^{-1}, 2 mmol l^{-1}, or 5 mmol l^{-1} unlabelled methylamine hydrochloride for 60 minutes. The incubation period was terminated by rinsing the oocytes in four washes of ice-cold standard OR2 with the same concentration of unlabelled methylamine as in the uptake buffer to remove any

external radioactivity. Individual oocytes were lysed in 200 µl of 10 % sodium dodecyl sulfate, followed by the addition of 3 ml of Ultima-Gold scintillation cocktail (PerkinElmer). Liquid scintillation spectrometry (Tri-Carb 2900 TR; PerkinElmer) was used to quantify the internal oocyte radioactivity as counts per minute (CPM) per oocyte.

2.6 *Statistical analysis*

All data sets are represented as the mean ± SEM, unless otherwise noted. A p-value of < 0.05 was considered significant. Statistical analyses and graphs were generated with GraphPad Prism 9.0 for Windows (GraphPad Software, San Diego, California USA, www.graphpad.com). Statistical analyses pertaining to each data set are described in the respective figure captions. Prior to analysis, data sets were tested for outliers using Grubb's test, and for normality (Shapiro-Wilk test) and homogeneity (Bartlett's test) for data sets assessed with a one-way ANOVA. Multiple comparisons were assessed with a post-hoc Tukey's pairwise comparisons test.

3.0 Results

3.1 Sequence analysis

Considering the scarcity of research on the HIAT1 transporter, no consistent nomenclature is available in the literature and many proteins available on NCBI are mistakenly annotated as different HIAT isoforms as a result of incorrectly assembled transcriptomes. Within our phylogenetic analysis, HIAT1 of arthropods (insects, crustaceans, and chelicerates) and vertebrates (fish and amphibians) are clearly separated into two distinct clades (Fig. 4). Among teleosts, three HIAT paralogues have been identified, HIAT1a, HIAT1-like and HIAT1b (Zhouyao et al., under review). It appears that the two HIAT1 isoforms discovered in *L. polyphemus* do not cluster with any of the 3 paralogues established in fish, prompting us to label

the newly discovered isoforms in the horseshoe crab as LpHIAT1α and LpHIAT1β. The open reading frames of LpHIAT1α (GenBank accession no. XP_013778555.1) and LpHIAT1β (GenBank accession no. XM_013929932.2) translate into a 509 and 494 amino acid protein, respectively. The two isoforms share an 82.7% conservation of identical amino acids. Genetic sequence analysis clearly distinguished LpHIAT1α and LpHIAT1β of *L. polyphemus* as separate isoforms, clustered most closely with *Ixodes scapularis* (deer tick) among other chelicerates (Fig. 4). When compared with *Trichoplax adhaerens*, a simple two-cell layer thick placozoan rooted at the base of the tree (Fig. 4), LpHIAT1α exhibits a 53% amino acid identity and 74% amino acid homology, indicating HIAT1 is highly conserved within the animal kingdom. Remarkably, the HIAT1 protein is even present in plants and fungi (Supplementary Table 2), suggesting that this protein must play a pivotal role in sustaining life of eukaryotic organisms.

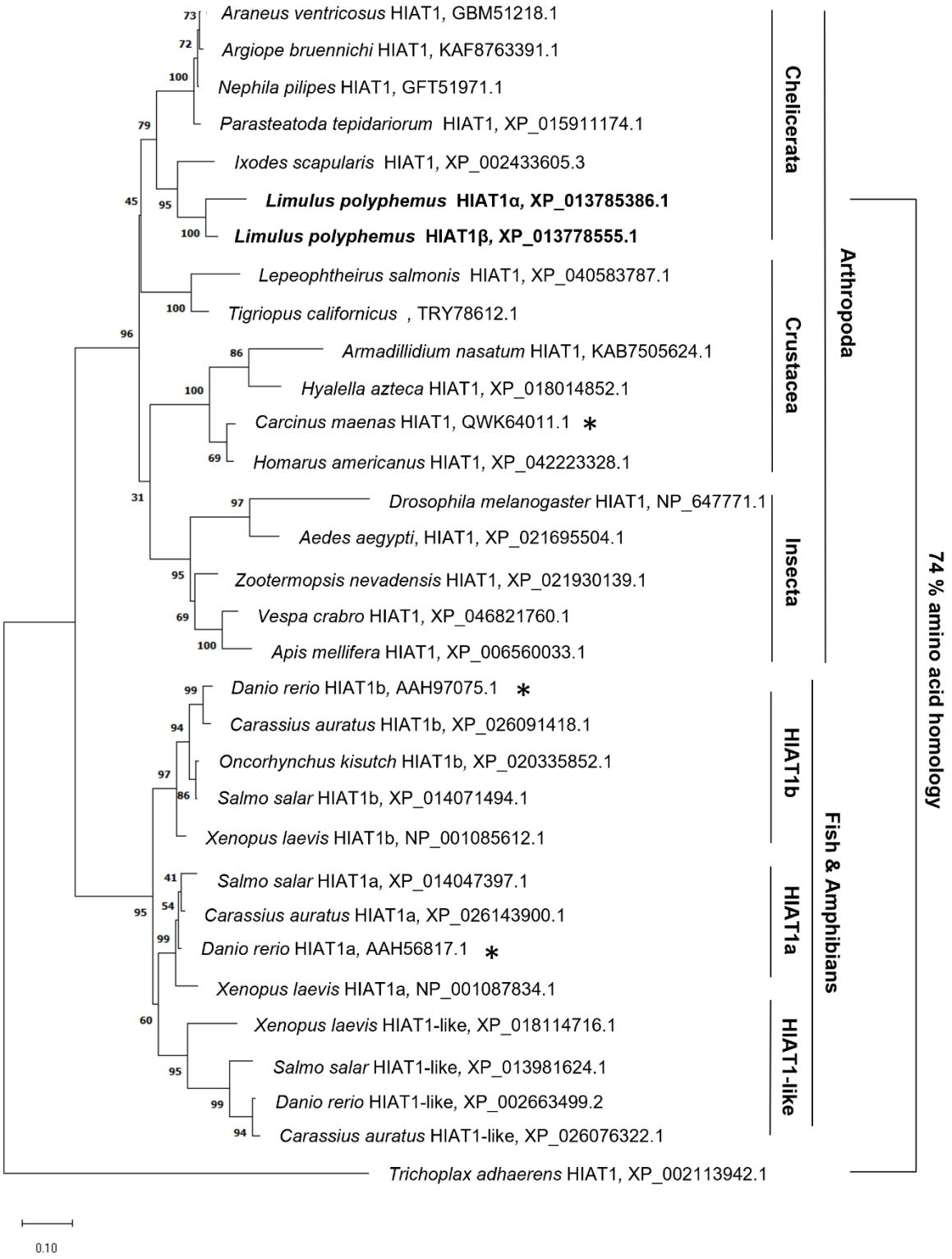

Figure 4. Genetic sequence analysis of the LpHIAT1α and LpHIAT1β isoforms identified in *Limulus polyphemus*. Represented is the maximum likelihood consensus tree of the MUSCLE alignment of HIAT1 protein performed with the MEGAX program. Numbers beside branches

represent bootstrap values (500 replicates). Percentages indicate the level of conservation between respective species (amino acid homology as determined by NCBI alignment). The tree is drawn to scale (as represented by the scale bar), with branch lengths measured in the number of substitutions per site. Stars (*) indicate species in which an ammonia transport function of the HIAT1 protein has been investigated previously to this study.

Structural analysis of LpHIAT1α and LpHIAT1β using Protter (Omasits et al., 2014) predicted 12 transmembrane domains (TMD) for both isoforms and a conserved sugar-binding motif within TMD3 at amino acid positions 95-102 (Fig. 5C). Both isoforms presented a predicted N-glycosylation motif at amino acids 61 and 418 (Fig. 5A and Fig. 5B), with LpHIAT1α presenting an additional motif at amino acid 223. All the N-glycosylation motifs were located on the amino acid asparagine (Asn). While both isoforms contained a predicted phosphoserine/threonine binding group at amino acid 124, LpHIAT1α contained an additional proline-dependent serine/threonine kinase group at amino acid 465 and an acidophilic serine/threonine kinase group at amino acid 476. The conserved sugar motif originally mentioned in mice by Matsuo et al. (1997) was also present in both *L. polyphemus* HIAT isoforms, as shown aligned with the motif regions in *H. sapiens* and *C. maenas* (Fig. 5C).

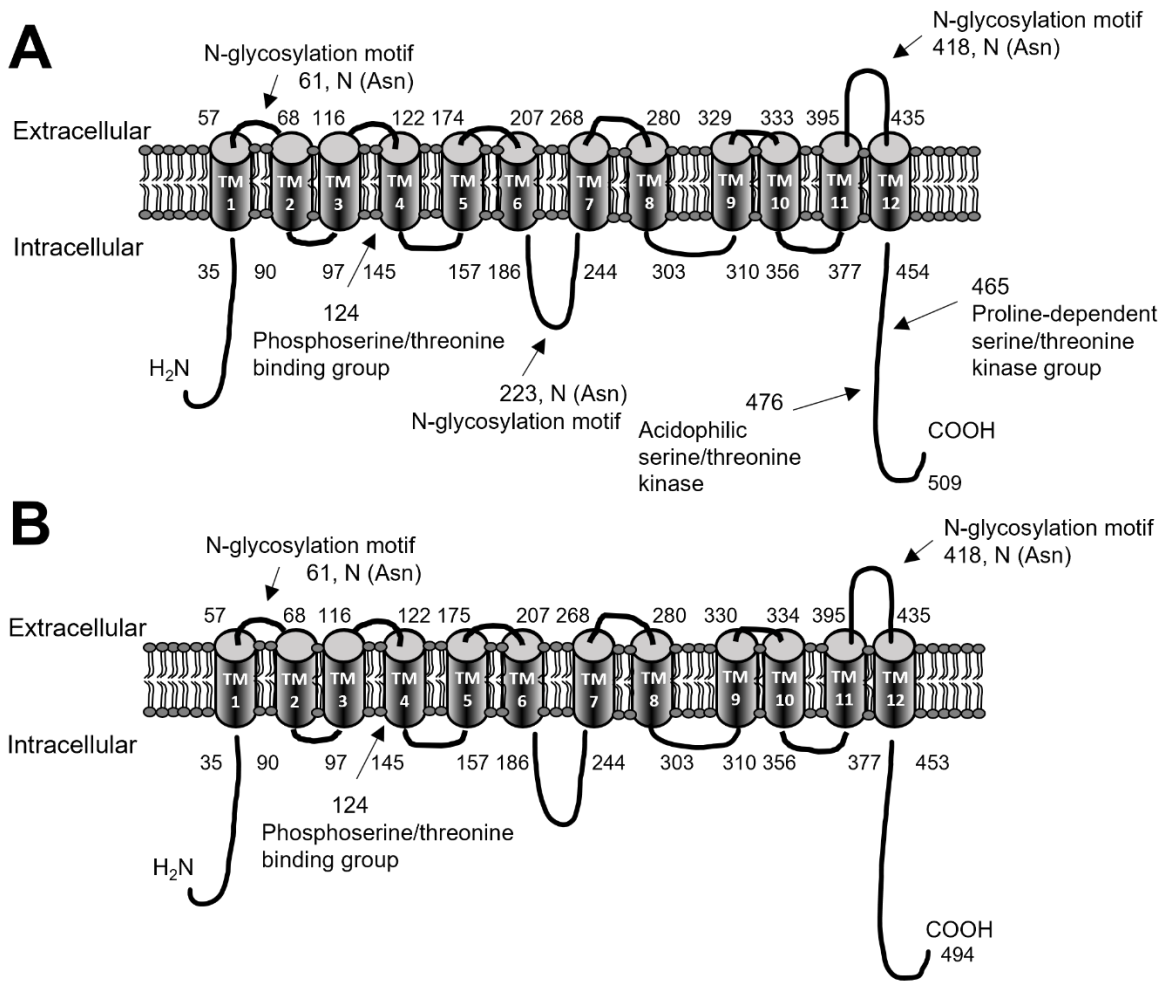

C

```
L. polyphemus HIAT1α   LSAPLVGALSDVWGRKVFLLLTVFFTCS
L. polyphemus HIAT1β   LSAPLVGALSDIWGRKVFLLLTVFFTCS
H. sapiens    MFSD14A  LSAPLIGALSDVWGRKSFLLLTVFFTCA
C. maenas     HIAT1    LSAPLIGALSDLWGRKFFLFITVFFTCL
```

Figure 5. Models of the 12 predicted transmembrane domains of the (**A**) LpHIAT1α and (**B**) LpHIAT1β isoforms identified in *L. polyphemus* (Protter, https://wlab.ethz.ch/protter). Arrows indicate predicted glycosylation sites (Protter, https://wlab.ethz.ch/protter) and predicted kinase motifs (Scansite 4.0, https://scansite4.mit.edu). (**C**) Amino acid alignment of the conserved sugar binding motif between *Limulus* HIAT1α and HIAT1β, and two species in which glucose transport by HIAT1 has been disproven (*Homo sapiens* HIAT1 and *Carcinus maenas* HIAT1).

3.2 Tissue expression

To analyze the tissue-specific expression of LpHIAT1α and LpHIAT1β, the relative mRNA abundance of both isoforms was evaluated by qPCR in ammonia excretory tissues (coxal gland, peripheral-mitochondria poor area (PMPA) and the central mitochondria-rich area (CMRA) of the gill) and the brain (circumesophageal neuropil ring), which may be sensitive to the effects of ammonia.

Both HIAT1 isoforms showed the significantly highest expression in the brain tissue compared to the coxal gland, PMPA and CMRA of the gill; with a 2.5-fold higher expression of LpHIAT1α and a 3.4-fold higher expression of LpHIAT1β in the brain compared to the PMPA (Fig. 6). The lowest expression of LpHIAT1β mRNA could be observed in the PMPA of the gill, whereas no difference in LpHIAT1α mRNA expression could be observed between the gill areas. Out of the two isoforms, LpHIAT1α was overall higher expressed in the brain, PMPA and CMRA of the gill compared to LpHIAT1β. The coxal gland showed an equal mRNA expression level of LpHIAT1α and LpHIAT1β (Fig. 6).

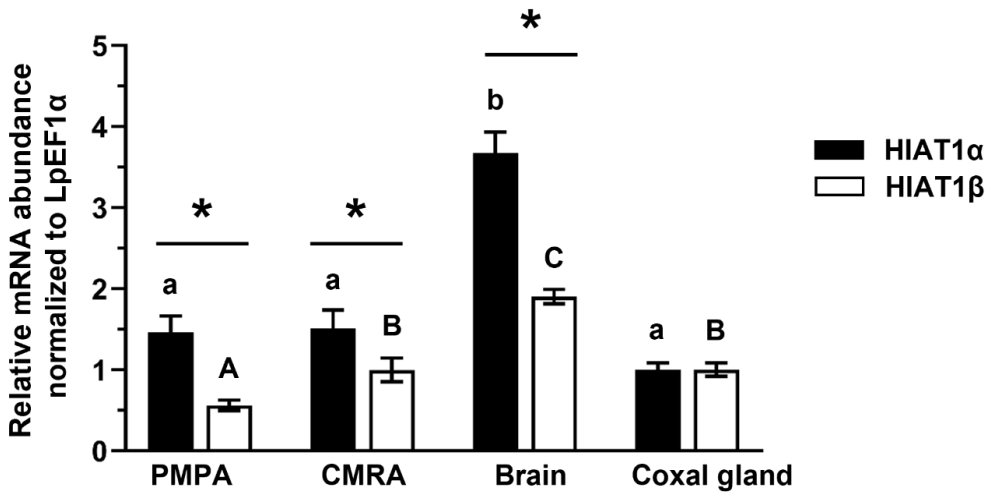

Figure 6. Relative mRNA abundance of LpHIAT1α (black bars) and LpHIAT1β (white bars) in the peripheral mitochondria-poor area (PMPA) of the gill, central mitochondria-rich area (CMRA) of the gill, brain, and coxal gland of *Limulus polyphemus*. All transcript levels are normalized relative to Elongation factor 1-alpha (LpEF1α) and shown as fold-differences of LpHIAT1α expression in the coxal gland (set to 1.0). Values are represented as mean ± SEM. Significant differences are denoted by lowercase letters for LpHIAT1α and uppercase letters for LpHIAT1β (Mixed-effects analysis with post-hoc Tukey's multiple comparisons test; $p < 0.05$; n = 5-6), whereas asterisk denote significant differences in mRNA abundance between LpHIAT1α and LpHIAT1β within each tissue (two-tailed t-test, $p < 0.05$; n = 5-6).

3.3 HIAT1 expression compared to other genes

In order to assess the importance of the HIAT1 transporter in the trans-branchial ammonia excretion process, the absolute mRNA expression levels of LpHIAT1α and LpHIAT1β were compared to other genes putatively involved in branchial ammonia excretion. Quantitative PCR analysis was performed on the dorsal and ventral gill-lamellar halves to identify potential gene expression differences in the epithelial layers.

In the dorsal and ventral gill halves of adult *L. polyphemus*, absolute mRNA expression of both HIAT isoforms was relatively low compared to the Na^+/K^+-ATPase α-subunit (NKA), V-type H^+-ATPase subunit B (HAT), cytoplasmic carbonic anhydrase (CA-2), Rhesus-protein 1 (Rh-1), and Rhesus-protein 2 (Rh-2) (Table 2). Striking and significant differences in the

expression of Rhesus-protein 1 (LpRh-1) compared to LpHIAT1α and LpHIAT1β could be observed, where in the ion-conductive ventral gill half, an approximately 127-fold and 159-fold higher expression of LpRh-1 expression could be observed compared to LpHIAT1α ($p < 0.0001$) and LpHIAT1β ($p < 0.0001$), respectively (Table 2).

Table 2. Absolute mRNA expression levels of genes putatively involved in ammonia excretion in *Limulus polyphemus*. Expression (copy numbers per ng of input total RNA) of LpHIAT1α, LpHIAT1β, Na^+/K^+-ATPase α-subunit (NKA), V-type H^+-ATPase subunit B (HAT), carbonic anhydrase isoform 2 (CA-2), Rhesus-protein 1 (Rh-1), and Rhesus-protein 2 (Rh-2) in adult *L. polyphemus* from control conditions. Values are represented as mean ± SEM. Significant differences are denoted by uppercase letters for the dorsal half-lamella and lowercase letters for the ventral half-lamella of the gill (log-transformed data was assessed by a one-way ANOVA with post-hoc Tukey's multiple comparisons test; $p < 0.05$; $n = 6$).

	LpHIAT1α	**LpHIAT1β**	**LpNKA**	**LpHAT**	**LpCA-2**	**LpRh-1**	**LpRh-2**
Mean ± SEM	*Dorsal* 47.76 ± 10.12 **BC**	*Dorsal* 29.00 ± 5.26 **C**	*Dorsal* 95.64 ± 30.26 **ABC**	*Dorsal* 200.3 ± 34.38 **ABC**	*Dorsal* 166.4 ± 89.0 **ABC**	*Dorsal* 454.7 ± 264.7 **AB**	*Dorsal* 271.8 ± 59.79 **A**
	Ventral 55.47 ± 8.45 **cd**	*Ventral* 44.63 ± 8.76 **c**	*Ventral* 103.3 ± 9.63 **cde**	*Ventral* 233.7 ± 38.1 **e**	*Ventral* 1,918.0 ± 505.2 **b**	*Ventral* 7,012 ± 1836 **a**	*Ventral* 178.7 ± 34.5 **de**
n	6	6	6	6	6	6	6

3.4 Acute HEA stress response

Horseshoe crabs were exposed to HEA (mean = 1,187 µmol l^{-1} NH_4Cl) over 24 hours to determine the effect of acute HEA stress on hemolymph ammonia levels. After 2 hours of HEA exposure, the mean hemolymph ammonia significantly increased 3.1-fold from 247.6 ± 27.1 µmol l^{-1} in control conditions to 767.1 ± 55.6 µmol l^{-1} (Fig. 7). Subsequent sampling points at T=6h and T=24h resulted in a stepwise 1.2-fold increase in hemolymph ammonia. After 24 hours of HEA exposure the animals' mean hemolymph ammonia concentration significantly increased

to 1,120.5 ± 70.5 µmol l^{-1}, nonetheless still below the mean tank ammonia concentration after 24 hours of HEA exposure, which was measured at 1,355.3 µmol $^{-1}$ (Fig. 7).

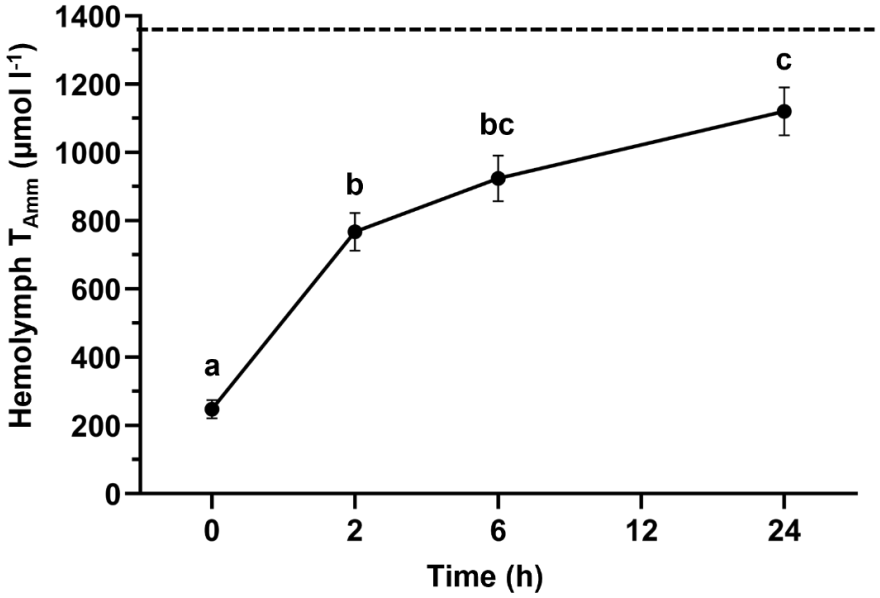

Figure 7. Hemolymph ammonia concentrations of *Limulus polyphemus* over a 24-hour HEA acclimation (1,187 µmol l^{-1} NH_4Cl). Hemolymph samples were taken at 0, 2, 6, 24 hours during HEA acclimation. Dotted line shows the mean tank NH_4Cl concentration of 1,355.3 µmol l^{-1} at T=24h. Values are represented as mean ± SEM. Significant differences in hemolymph ammonia concentration between sampling points are denoted by lowercase letters (one-way ANOVA with post-hoc Tukey's multiple comparisons test; $p < 0.05$; $n = 8$).

3.5 Effect of acute HEA stress on gene expression

To determine the role of genes putatively involved in branchial ammonia excretion during acute HEA stress, the relative mRNA abundance of LpHIAT1α, LpHIAT1β, NKA, CA-2, HAT, Rh-1, and Rh-2 was assessed in the dorsal and ventral gill halves of adult *L. polyphemus* exposed to 1 mmol l^{-1} NH_4Cl for 24 hours. No significant differences in gene expression could be observed for any of the above-mentioned transporters in the dorsal gill half after a 24-hour HEA stress (Fig. 8A), whereas a significant 1.3-fold increase in the relative mRNA expression of LpHIAT1β could be observed in the ventral gill half (Fig. 8B).

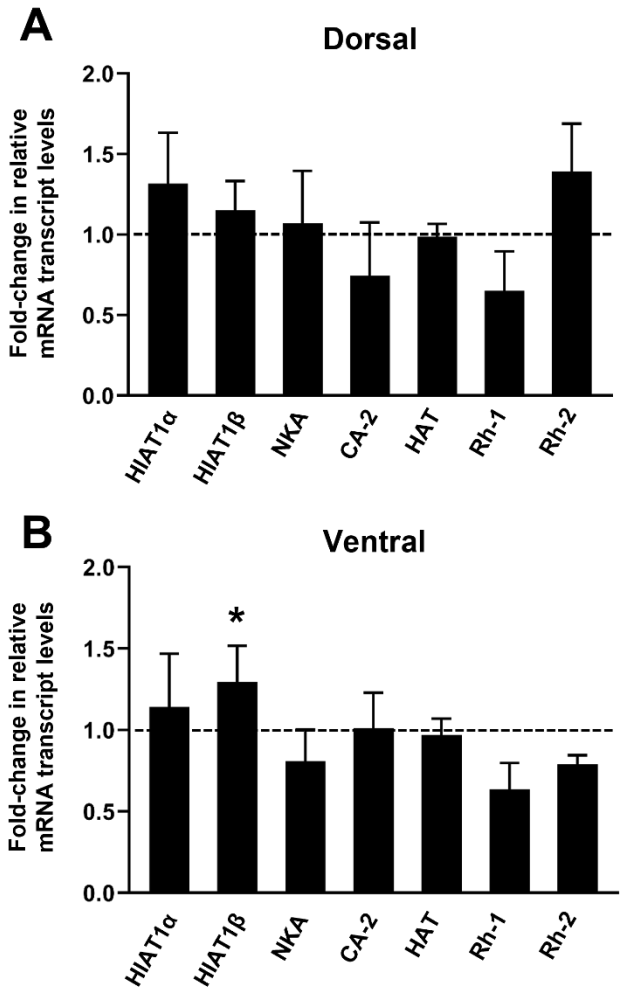

Figure 8. Effect of acute HEA stress on mRNA transcript levels in the Dorsal (**A**) and Ventral (**B**) gill halves. Transcript levels after acute (24 h) acclimation of adult *L. polyphemus* to high environmental ammonia of 1 mmol l^{-1} (HEA). Values are represented as mean ± SEM. Transcript levels are normalized relative to Elongation factor 1-alpha (LpEF1α) and shown as fold-changes relative to their expression under control conditions (set to 1.0). Significant differences between control and treatment are denoted by asterisk (paired two-tailed t-test; $p < 0.05$; $n = 6$).

3.6 Effect of short-term HEA and hypercapnia acclimation on LpHIAT1α and LpHIAT1β gene expression

Ammonia excretion is often associated with the maintenance of acid-base balance, possibly by virtue of ammonia's ability to act as a weak base and bind excess H^+, and several key transporters are shared by both processes (Fehsenfeld and Weihrauch, 2016). This prompted us to investigate the effect of elevated pCO_2 conditions on the HIAT1 transporter in the branchial regions of *L. polyphemus*. The effect of a short-term (7-9 day) acclimation to either 1 mmol l^{-1} NH_4Cl (HEA) or 300 Pa CO_2 (high pCO_2) on LpHIAT1α and LpHIAT1β mRNA transcript abundance in the dorsal and ventral gill halves was assessed by qPCR. No change in relative LpHIAT1α mRNA expression could be observed in the dorsal or ventral gill halves in response to either treatment (Fig. 9A). However, a 1.4-fold higher expression of LpHIAT1β could be observed in the ion-conductive ventral gill half after the short-term HEA treatment (Fig. 9B).

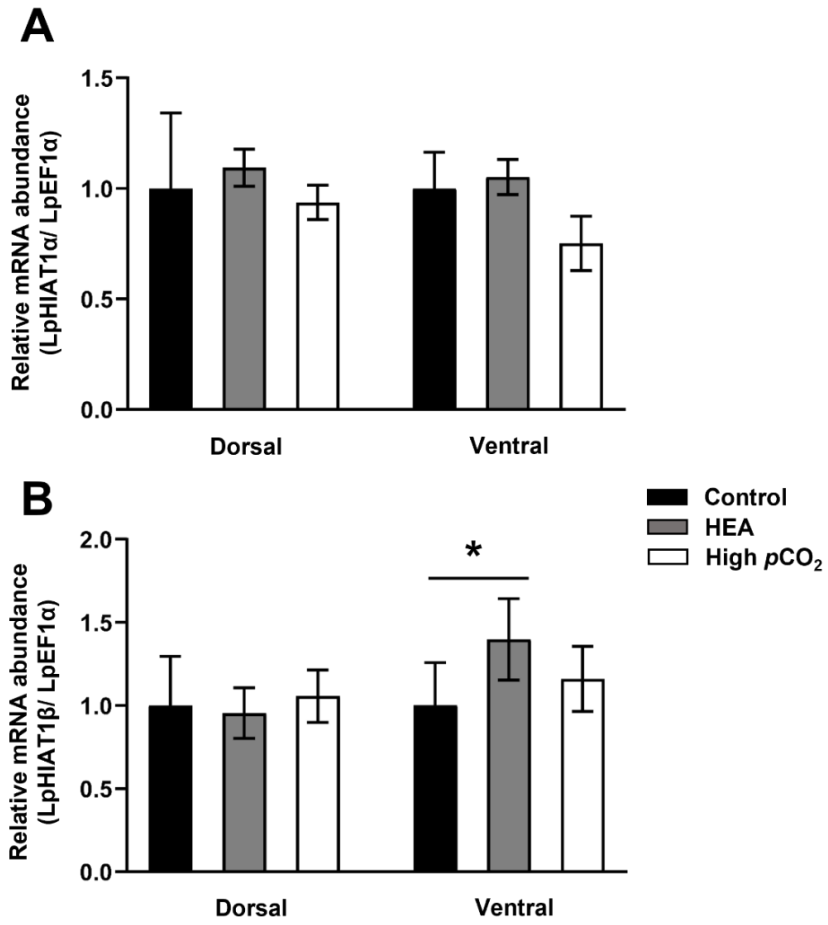

Figure 9. Relative mRNA abundance of **(A)** LpHIAT1α and (**B**) LpHIAT1β in *Limulus polyphemus* dorsal and ventral gill regions halves after high-environmental ammonia and hypercapnia treatment. Transcript levels are normalized relative to Elongation factor 1-alpha (LpEF1α) and shown as fold-differences of the Control (black bars, set to 1.0). Grey bars represent mRNA abundance after a short-term (7-9 days) acclimation of adult *L. polyphemus* to high environmental ammonia of 1 mmol l^{-1} (HEA), whereas white bars represent a 7-9 day acclimation to 300 Pa CO_2 (high pCO_2). Values are represented as mean ± SEM. Significant differences between control and treatments are denoted by asterisk (two-tailed t-test; $p < 0.05$; n = 5-6).

3.7 ^{3}H-methylamine uptake mediated by LpHIAT1α and LpHIAT1β expressed in Xenopus laevis oocytes

Sham-injected oocytes mediated a ^{3}H-methylamine uptake of approximately 163 pmol oocyte^{-1} h^{-1} at a 1 mmol l^{-1} background level of unlabeled methylamine (MA) (Fig. 10A). Oocytes expressing LpHIAT1α and LpHIAT1β showed a significantly lower uptake of methylamine (approximately 29 % and 25 % respectively) in comparison to the Sham control under the same conditions. When exposed to a 2 mmol l^{-1} methylamine concentration, LpHIAT1α-expressing oocytes maintained an approximately 25 % lower uptake rate than the Sham oocytes, whereas LpHIAT1β-expressing oocytes failed to maintain a lower uptake (Fig. 10B). At a background methylamine concentration of 5 mmol l^{-1}, both LpHIAT1α-expressing and LpHIAT1β-expressing oocytes failed to maintain a lower methylamine uptake, with both reaching roughly equal methylamine uptake rates as the Sham control oocytes (Fig. 10C).

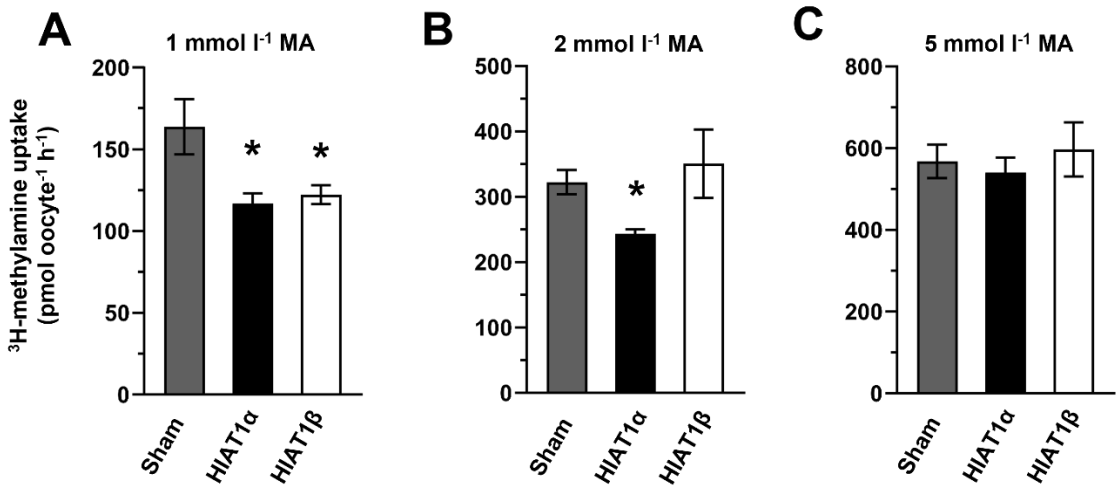

Figure 10. Methylamine flux studies in *Xenopus laevis* oocytes expressing LpHIAT1α and LpHIAT1β at varying methylamine background concentrations. Absolute ^{3}H-methylamine (radioactive-labelled) uptake of sham-injected, LpHIAT1α-injected and LpHIAT1β-injected oocytes at unlabeled methylamine (MA) concentrations of **(A)** 1 mmol l^{-1}, **(B)** 2 mmol l^{-1}, and **(C)** 5 mmol l^{-1} after a 60-minute incubation (pH 7.5). Asterisk indicates significant differences in uptake between Sham controls and LpHIAT1α- and LpHIAT1β-injected oocytes (two-tailed t-test; $p < 0.05$; $n = 9$). Values are presented as means ± SEM.

4.0 Discussion

A recent characterization of the HIAT1 protein as a novel ammonia transporter in teleosts has influenced further characterization and functional studies of this protein in other animal systems, particularly due to its high conservation among the animal kingdom and the implications on cellular homeostasis (Zhouyao et al., under review). This study presents the first characterization of two distinct isoforms of this novel ammonia transporter, LpHIAT1α and LpHIAT1β, in the morphologically ancient marine chelicerate *Limulus polyphemus*.

To date, one isoform of HIAT1 has been identified in invertebrates/crustaceans (Fehsenfeld et al., personal communication), and 3 paralogues (HIAT1a, HIAT1b, Hiat1-like) have been identified in fish (Zhouyao et al., under review). The DrHiat1b paralogue in zebrafish is distinguished as the only paralogue with the presence of a proline-dependent serine/threonine kinase group at amino acid section 456-469. Interestingly, the HIAT1α isoform of *L. polyphemus* presented in this study contains the same predicted proline-dependent serine/threonine kinase group at amino acid number 465 (Fig. 5A), this group is however missing in the HIAT1β isoform of *L. polyphemus*. Phosphorylated proline-dependent serine/threonine sites serve as binding motifs to recruit proteins into signalling networks or placing enzymes closer to substrates, and regulate protein function by means of conformational changes (Jha et al., 2006; Pawson and Scott, 1997). The differences in glycosylation motifs and phosphorylation sites suggest potential and yet unknown functional differences between the LpHIAT1α and LpHIAT1β isoforms.

The sugar binding motif between TMD 2-3 remains conserved among both HIAT1 isoforms in *L. polyphemus*, as well as across the animal kingdom (*C. maenas, D. rerio, Mus*

musculus, *H. sapiens*; Fig. 5C). Originally, a glucose transport function has been suggested solely based on the presence of this conserved sugar binding motif (Matsuo et al., 1997), but was disproven when functional studies in oocytes expressing the HIAT1 protein of humans and the green crab did not facilitate the transport of ^{3}H-2-deoxyglucose (Zhouyao et al., 2022; Fehsenfeld et al., personal communication). Due to the high conservation of amino acid identity in the sugar binding motif across the animal kingdom (88 % amino acid identity between *L. polyphemus* HIAT1α and *Homo sapiens* (here termed MFSD14a)), we assume that, similar to humans and crustaceans, LpHIAT1α and LpHIAT1β also do not serve a glucose transport function in *L. polyphemus*. Future experiments, however, still have to confirm this assumption.

To verify the hypothesis that LpHIAT1α and LpHIAT1β transport ammonia, we completed indirect flux experiments in *Xenopus laevis* oocytes utilizing the established radiolabeled ammonia analogue ^{3}H-methylamine. To interpret the flux studies conducted in this investigation, it is noteworthy that *X. laevis* oocytes endogenously express a XlHIAT1 protein (Fehsenfeld et al., personal communication). This substantiates the importance of this transporter in the earliest stages of life, presumably by ensuring homeostasis in the one-cell stadium, but needs to be considered as a potential source of uncertainty. Additionally, *X. laevis* oocytes endogenously express very low levels of an Rh-protein, Rhag (Fehsenfeld et al., personal communication), which may mediate methylamine transport (Nakada et al., 2007). While unprotonated methylamine may enter the oocyte along its partial pressure gradient *via* diffusion across the lipid bilayer, the flux is presumably very small with 0.00079 % of unprotonated methylamine (ca. 0.8 µmol at a background methylamine concentration of 1 mmol) existing at an experimental pH of 7.5 with methylamine's pKa of 10.6. These passive fluxes and the endogenous expression of ammonia transporters may contribute to methylamine and/or ammonia

uptake, as observed in the background methylamine uptake rate of around 163 pmol oocyte^{-1} h^{-1} for control (Sham) oocytes (Fig. 10A, Sham). Considering that these endogenous methylamine and/or ammonia pathways of the frog oocytes affect the background methylamine uptake rates of Sham- and HIAT1-oocytes to the same extent, we observed that oocyte expression of both isoforms, LpHIAT1α and LpHIAT1β, promoted a significantly lower methylamine uptake than water-injected Sham controls when subjected to 1 mmol l^{-1} methylamine (Fig. 10A). This finding indicates that an over-expression of both *Limulus* HIAT1 isoforms promotes, by a so far unknown mechanism, not an uptake but an excretion of methylamine out of the oocyte and therefore likely also an ammonia excretion. An increase of the methylamine concentration in the incubation buffer from 1 mmol l^{-1} to 2 mmol l^{-1} resulted in a proximate duplication of the ^{3}H-methylamine uptake rates into Sham oocytes. While the expression of LpHIAT1α in the oocytes resulted in a reduced uptake at this increased background methylamine concentration, no difference in uptake rates between LpHIAT1β-expressing and Sham oocytes could be observed, indicative of different substrate affinities and transport capabilities between these two isoforms. The substantially higher methylamine concentration in the incubation media has to be considered. At the 60-minute incubation sampling point, a roughly 6.5-fold inward-directed gradient of methylamine can be calculated assuming an oocyte volume of ca. 1 µl (Parisis, 2020). The lack of methylamine excretion for both transporters at a 5 mmol l^{-1} methylamine background concentration might be due to the now ca. 9-fold inward-directed gradient of methylamine, which presumably cannot be conquered anymore.

The potential differences in chemical properties between methylamine and ammonia, and therefore potential differences in substrate specificity and/or transport mechanisms, also need to be considered. Our indirect ammonia excretion results are substantiated by the observation of a

higher NH_3/NH_4^+ excretion in oocytes expressing a crustacean HIAT1 protein (*C. maenas*; CmHIAT1), measured directly using SIET (Scanning Ion-Selective Electrode Technique) experiments employing NH_4^+-selective electrodes. This ammonia excretion was dependent on the presence of Na^+ cations in the incubation solution, suggesting a secondary active Na^+/NH_4^+ exchange mechanism (Fehsenfeld et al., personal communication). Similar results were observed in *D. rerio* larvae, where a significant reduction in NH_4^+ flux was observed using SIET in DrHiat1b knockout larvae (Zhouyao et al., under review). Further experiments are required to explore the actual substrate specificities, nature, and kinetics of these transporters.

The evidence that both LpHIAT1α and LpHIAT1β promote a methylamine transport led to the speculation that these transporters may be involved in branchial ammonia excretion processes in the horseshoe crab. This hypothesis was fueled by the findings in zebrafish (*D. rerio*). Here, knockdown of one of the paralogues (DrHiat1b) resulted in an 85% reduced ammonia excretion rate at the excretory sites (yolk sac and immature gill/pharyngeal region) (Zhouyao et al., under review).

A tissue expression analysis in *L. polyphemus* demonstrated mRNA expression of both isoforms in the peripheral mitochondria poor area (PMPA) and the central mitochondria rich area (CMRA) of the gill, however the overall abundance was significantly higher in the brain (prosomal circumesophageal neuropil ring; see Fig. 6). Interestingly, a unique characteristic of the horseshoe crab is its brain, which is largely enclosed within arterial vessels (Dumont et al., 1965) and the absence of any internal cellular lining. Hence, the arterial muscular walls serve as the neural lamella and provide the only diffusional barrier in the brain (Fahrenbach, 1976), which may increase the brain's sensitivity to elevated ammonia levels present in the animal's hemolymph. The relatively high mRNA expression of the two HIAT1 isoforms in the brain of *L.*

polyphemus compared to the excretory gill tissues, indicates an ammonia-protective function of the transporters, likely in the form of ammonia excretion for cellular detoxification. Similar to the endogenous expression of XlHIAT in the single-cell *X. laevis* oocytes mentioned earlier, the zebrafish HIAT1 paralogues DrHiat1a and DrHiat1b were also maternally expressed and showed an early onset of transcription in the maternal-to-zygotic transition of the developing *D. rerio* embryo (Zhouyao et al., under review). The expression of DrHiat1a and DrHiat1b was mainly localized to the head/brain region 24 hours post-fertilization (Zhouyao et al., under review). Comparably, high expression of the HIAT1/MFSD14A protein was first discovered in the neonatal mouse hippocampus (Matsuo et al., 1997), emphasizing the importance of the HIAT transporter as a potential ammonia transporter in the early stages of development and in the nervous system across the animal kingdom.

When compared to other enzymes and transporters often involved in ammonia excretion processes and/or acid-base regulation, such as the Na^+/K^+-ATPase, V-type H^+ -ATPase, and Rh-proteins (Adlimoghaddam et al., 2015; Hans et al., 2018; Larsen et al., 2014; Martin et al., 2011b; Masui et al., 2003; Nawata et al., 2010; Quijada-Rodriguez et al., 2015; Thiel et al., 2017; Weihrauch et al., 2002, 1998), absolute mRNA expression levels of LpHIAT1α and LpHIAT1β were the lowest (Table 2). In addition, the LpHIAT1α isoform showed an equal expression strength in the CMRA and PMPA of the gill, comparable to the expression pattern found for the Na^+/K^+-ATPase, the pump that, in theory could energize HIAT1 (Hans et al., 2018). This is in stark contrast to the branchial expression found for the Rh-proteins, channels known to be involved in ammonia excretion processes in invertebrates, fish and mammals (Adlimoghaddam et al., 2015; Marini et al., 2000; Martin et al., 2011b; Nawata et al., 2010; Quijada-Rodriguez et al., 2015). While LpRh-1 showed a ca. 20-folds higher expression strength in the CMRA when

compared to the PMPA of the gill, LpRh-2 was higher (ca. 2-fold) expressed in PMPA (Hans et al., 2018). It should be noted that mRNA expression levels do not necessarily equate with protein abundance, and that qPCR results in this study are rather interpreted as an indication of the protein's importance. These findings suggest that the HIAT1 transporters serve a fundamental function in the horseshoe crab, as indicated by the ubiquitous tissue expression pattern (see Fig. 6), but are likely not as imperative to the trans-branchial ammonia excretion mechanism as to the extent documented for the Rh-proteins (Martin et al., 2011b; Si et al., 2018; Weihrauch et al., 2004; Wright and Wood, 2009). Nonetheless, both LpHIAT1α and LpHIAT1β are expressed to a certain high degree (ca. 50 % of transcript abundance compared to the α-subunit of the Na^+/K^+-ATPase) in the dorsal and ventral side of the gill (see Table 2; Hans et al., 2018).

Horseshoe crabs often bury themselves in the sediment when foraging or hiding, and emerge to beaches and fluctuating estuarine areas during their seasonal mating migration (Brockmann, 1990). These circumstances may expose the animals to HEA and elevated pCO_2 conditions on a regular basis, as a result of metabolic waste accumulation and low water circulation (McGaw, 2005). To test, whether the LpHIAT1 isoforms are involved in mediating the effects of acute HEA exposure, animals were subjected to 1 mmol l^{-1} NH_4Cl for 24 hours. Within this time period, the animals accumulated ammonia to environmental concentrations (see Fig. 7). This acute acclimation did not induce any changes in mRNA transcript abundance of proteins commonly involved in branchial ammonia excretion (NKA, CA-2, HAT, Rh-1, Rh-2) (see Fig. 8), suggesting that the animals were able to tolerate an acute HEA stress without the need to regulate gene expression yet. Previous research on ammonia excretion in *L. polyphemus* demonstrated that hemolymph ammonia concentrations were adjusted back to control levels (334.0 ± 28.3 μmol l^{-1}; Hans et al., 2018) during a rather chronic acclimation (7-9 days) to HEA,

accompanied by an increased ammonia excretion rate and an upregulation of CA-2, HAT, and HCN mRNA transcripts in the ventral half-lamella, as well as an upregulation of CA-2 and Rh-1 mRNA transcripts in the dorsal half-lamella. In the current study, an increase in mRNA expression of LpHIAT1β could be detected in the ventral half-lamella after the acute (24 h) HEA stress (Fig. 8B), which also remained elevated after 7-9 days of HEA exposure (Fig. 9B). In contrast, mRNA expression levels of LpHIAT1α were unaffected by HEA, suggesting once again a different, yet unknown, function for these two isoforms.

A 7-9 day exposure to ca. 300 Pascals pCO_2 (pH = 7.4) did not cause any changes in mRNA expression levels of LpHIAT1α and LpHIAT1β in the gills of the horseshoe crab, suggesting that LpHIAT1α and LpHIAT1β are presumably not directly involved in cellular pH homeostasis in the gills of the horseshoe crab. However, it must be noted that in an earlier study on horseshoe crab gills, the same conditions only affected the V-type H^+-ATPase located on the ventral half-lamella (HAT, ca. 50 % upregulation) and did not affect other genes commonly involved in acid-base homeostasis or ammonia excretion, such as the Rh-proteins, NKA, CA-2 and HCN (Hans et al., 2018). Since hypercapnia treatment resulted in a significant increase in hemolymph pCO_2 levels (301.7 ± 33.7 Pa) but no change in hemolymph pH (pH 7.62 ± 0.05), it has been suggested that the respiratory acidosis was likely compensated by the action of the V-type H^+-ATPase (Hans et al., 2018).

On the contrary, a significant down-regulation of CmHIAT1 was observed in *C. maenas* in response to a 7-day hypercapnia exposure (Fehsenfeld et al., 2011, falsely annotated as hyperpolarization-activated nucleotide-gated Na^+/K^+-channel in the cited publication). This could be a result of the differences in acid-base buffering mechanisms used by the two species – exposure to hypercapnia in *C. maenas* resulted in elevated hemolymph ammonia levels and a

downregulation in ammonia transport pathways (CmHIAT1,Fehsenfeld et al., 2011; Rh-protein, Fehsenfeld and Weihrauch, 2013), whereas a significant reduction in hemolymph ammonia could be observed in *L. polyphemus* (Hans et al., 2018), which could explain the unresponsiveness of proteins involved in ammonia transport.

5.0 Conclusion

This study is the first to identify an ammonia transport function of two distinct isoforms of the highly conserved HIAT1 transporter, LpHIAT1α and LpHIAT1β, in the marine chelicerate *Limulus polyphemus* (American horseshoe crab). Considering the differences in glycosylation motifs, phosphorylation sites, mRNA abundance, and methylamine-transport capabilities, LpHIAT1α and LpHIAT1β can be clearly distinguished as two different isoforms. Further research on the characterization of these transporters would benefit from the cellular localization and enzyme kinetics of both isoforms to justify the presence and need of two isoforms in this organism. The high mRNA expression of both isoforms in the brain suggests a protective function of the HIAT1 transporter in horseshoe crabs, likely in the form of cellular ammonia detoxification, as supported by the LpHIAT1α- and LpHIAT1β-facilitated excretion of the radiolabeled ammonia analogue ^{3}H-methylamine in *X. laevis* oocytes. This might also prove important in fertility, as HIAT1-mutant mice presented with malformed spermatozoa and sterility (Doran et al., 2016). The role of LpHIAT1α and LpHIAT1β in ammonia protection of the brain and reproductive system (gonads) *via* gene knockdown studies needs to be investigated further.

6.0 References

Adlimoghaddam, A., Boeckstaens, M., Marini, A.M., Treberg, J.R., Brassinga, A.K.C., Weihrauch, D., 2015. Ammonia excretion in Caenorhabditis elegans: Mechanism and evidence of ammonia transport of the Rhesus protein CeRhr-1. J. Exp. Biol. 218, 675–683. https://doi.org/10.1242/jeb.111856

Avise, J.C., Nelson, W.S., Sugita, H., 1994. A Speciational History of "Living Fossils": Molecular Evolutionary Patterns in Horseshoe Crabs. Evolution (N. Y). 48, 1986. https://doi.org/10.2307/2410522

Braissant, O., McLin, V.A., Cudalbu, C., 2013. Ammonia toxicity to the brain. J. Inherit. Metab. Dis. 36, 595–612. https://doi.org/10.1007/s10545-012-9546-2

Brockmann, H.J., 1990. Mating Behavior of Horseshoe Crabs , Limulus polyphemus. Behaviour 114, 206–220.

Brody, T. (1999). Protein. In T. Brody, Nutritional Biochemistry (pp. 421-489). University of California at Berkeley Berkeley, California: Elsevier Inc.

Butterworth, R.F., 2002. Pathophysiology of hepatic encephalopathy: A new look Ammonia. Metab. Brain Dis. 17, 221–227. https://doi.org/10.1023/B:MEBR.0000043979.58915.41

Caldeira, K., Wickett, M., 2005. Ocean model predictions of chemistry changes from carbon dioxide emissions to the atmosphere and ocean. J. Geophys. Res. C Ocean. 110, 1–12. https://doi.org/10.1029/2004JC002671

Cameron, J.N., Heisler, N., 1983. Studies of Ammonia in the Rainbow Trout:Physico-chemical Parameters, Acid-Base Behaviour and Respiratory Clearance. J. Exp. Biol. 105, 107–125. https://doi.org/10.1242/jeb.105.1.107

Chasiotis, H., Ionescu, A., Misyura, L., Bui, P., Fazio, K., Wang, J., Patrick, M., Weihrauch, D., Donini, A., 2016. An animal homolog of plant Mep/Amt transporters promotes ammonia excretion by the anal papillae of the disease vector mosquito Aedes aegypti. J. Exp. Biol. 219, 1346–1355. https://doi.org/10.1242/jeb.134494

Choe, H., Sackin, H., Palmer, L.G., 2000. Permeation properties of inward-rectifier potassium channels and their molecular determinants. J. Gen. Physiol. 115, 391–404. https://doi.org/10.1085/jgp.115.4.391

Cooper, A.J.L., Plum, F., 1987. Biochemistry and physiology of brain ammonia. Physiol. Rev. 67, 440–519. https://doi.org/10.1152/physrev.1987.67.2.440

Doran, J., Walters, C., Kyle, V., Wooding, P., Hammett-Burke, R., Colledge, W.H., 2016. Mfsd14a (Hiat1) gene disruption causes globozoospermia and infertility in male mice. Reproduction 152, 91–99. https://doi.org/10.1530/REP-15-0557

Durant, A.C., Donini, A., 2020. Ammonium transporter expression in sperm of the disease vector Aedes aegypti mosquito influences male fertility. Proc. Natl. Acad. Sci. U. S. A. 117, 29712–29719. https://doi.org/10.1073/pnas.2011648117

Durant, A.C., Donini, A., 2018. Ammonia excretion in an osmoregulatory syncytium is facilitated by AeAmt2, a novel ammonia transporter in aedes aegypti larvae. Front. Physiol. 9, 1–16. https://doi.org/10.3389/fphys.2018.00339

Eddy, F.B., 2005. Ammonia in estuaries and effects on fish. J. Fish Biol. https://doi.org/10.1111/j.1095-8649.2005.00930.x

Elin, R.J., Wolff, S.M., 1973. Nonspecificity of the limulus amebocyte lysate test: Positive reactions with polynucleotides and proteins. J. Infect. Dis. 128, 349–352. https://doi.org/10.1093/infdis/128.3.349

Fehsenfeld, S., Kiko, R., Appelhans, Y., Towle, D.W., Zimmer, M., Melzner, F., 2011. Effects of elevated seawater pCO2on gene expression patterns in the gills of the green crab, Carcinus maenas. BMC Genomics 12. https://doi.org/10.1186/1471-2164-12-488

Fehsenfeld, S., Weihrauch, D., 2016. The role of an ancestral hyperpolarization-activated cyclic + nucleotide-gated K channel in branchial acid-base regulation in the green crab, Carcinus maenas. J. Exp. Biol. 219, 887–896. https://doi.org/10.1242/jeb.134502

Fehsenfeld, S., Wood, C.M., 2020. A potential role for hyperpolarization-activated cyclic nucleotide-gated sodium/potassium channels (HCNs) in teleost acid-base and ammonia regulation. Comp. Biochem. Physiol. Part - B Biochem. Mol. Biol. 248–249, 110469. https://doi.org/10.1016/j.cbpb.2020.110469

Hans, S., 2016. Acid-Base Regulation and Ammonia Excretion in the American Horseshoe Crab , Limulus polyphemus. University of Manitoba.

Hans, S., Quijada-Rodriguez, A.R., Allen, G.J.P., Onken, H., Treberg, J.R., Weihrauch, D., 2018. Ammonia excretion and acid-base regulation in the American horseshoe crab, Limulus polyphemus. J. Exp. Biol. 221, 1–13. https://doi.org/10.1242/jeb.151894

Henry, R.P., Gehnrich, S., Weihrauch, D., Towle, D.W., 2003. Salinity-mediated carbonic anhydrase induction in the gills of the euryhaline green crab, Carcinus maenas. Comp. Biochem. Physiol. - A Mol. Integr. Physiol. 136, 243–258. https://doi.org/10.1016/S1095-6433(03)00113-2

Henry, R.P., Jackson, S.A., Mangum, C.P., 1996. Ultrastructure and transport-related enzymes of the gills and coxal gland of the horseshoe crab Limulus polyphemus. Biol. Bull. 191, 241–250. https://doi.org/10.2307/1542927

Henry, R.P., Wang, Y., Wood, C.M., 1997. Carbonic anhydrase facilitates CO2 and NH3 transport across the sarcolemma of trout white muscle. Am. J. Physiol. - Regul. Integr. Comp. Physiol. 272. https://doi.org/10.1152/ajpregu.1997.272.6.r1754

Hu, M.Y., Sung, P.H., Guh, Y.J., Lee, J.R., Hwang, P.P., Weihrauch, D., Tseng, Y.C., 2017. Perfused gills reveal fundamental principles of pH regulation and ammonia homeostasis in the cephalopod Octopus vulgaris. Front. Physiol. 8. https://doi.org/10.3389/fphys.2017.00162

Jha, K.N., Salicioni, A.M., Arcelay, E., Chertihin, O., Kumari, S., Herr, J.C., Visconti, P.E., 2006. Evidence for the involvement of proline-directed serine/threonine phosphorylation in sperm capacitation. Mol. Hum. Reprod. 12, 781–789. https://doi.org/10.1093/molehr/gal085

Jones D.T., Taylor W.R., and T.J.M., 1992. The rapid generation of mutation data matrices from protein sequences. e. Comput. Appl. Biosci. 8, 275–282.

Klymasz-Swartz, A.K., Allen, G.J.P., Treberg, J.R., Yoon, G.R., Tripp, A., Quijada-Rodriguez, A.R., Weihrauch, D., 2019. Impact of climate change on the American lobster (Homarus americanus): Physiological responses to combined exposure of elevated temperature and pCO2. Comp. Biochem. Physiol. -Part A Mol. Integr. Physiol. 235, 202–210. https://doi.org/10.1016/j.cbpa.2019.06.005

Kumar S., Stecher G., Li M., Knyaz C., and T.K., 2018. MEGA X: Molecular Evolutionary Genetics Analysis across computing platforms. Mol. Biol. Evol. 35, 1547–1549.

Larsen, E.H., Deaton, L.E., Onken, H., O'Donnell, M., Grosell, M., Dantzler, W.H., Weihrauch, D., 2014. Osmoregulation and excretion. Compr. Physiol. 4, 405–573. https://doi.org/10.1002/cphy.c130004

Lekholm, E., Perland, E., Eriksson, M.M., Hellsten, S. V., Lindberg, F.A., Rostami, J., Fredriksson, R., 2017. Putative membrane-bound transporters MFSD14A and MFSD14B are neuronal and affected by nutrient availability. Front. Mol. Neurosci. 10, 1–13. https://doi.org/10.3389/fnmol.2017.00011

Mangum, C.P., Booth, C.E., DeFur, P.L., Heckel, N.A., Henry, R.P., Oglesby, L.C., Polites, G., 1976. The ionic environment of hemocyanin in Limulus polyphemus. Biol. Bull. 150, 453–467. https://doi.org/10.2307/1540685

Marcaida, G., Felipo, V., Hermenegildo, C., Miñana, M.D., Grisolia, S., 1992. Acute ammonia toxicity is mediated by the NMDA type of glutamate receptors. FEBS Lett. 296, 67–68. https://doi.org/10.1016/0014-5793(92)80404-5

Marini, A.M., Matassi, G., Raynal, V., André, B., Cartron, J.P., Chérif-Zahar, B., 2000. The human Rhesus-associated RhAG protein and a kidney homologue promote ammonium transport in yeast. Nat. Genet. 26, 341–344. https://doi.org/10.1038/81656

Martin, M., Fehsenfeld, S., Sourial, M.M., Weihrauch, D., 2011a. Effects of high environmental ammonia on branchial ammonia excretion rates and tissue Rh-protein mRNA expression levels in seawater acclimated Dungeness crab Metacarcinus magister. Comp. Biochem. Physiol. - A Mol. Integr. Physiol. 160, 267–277. https://doi.org/10.1016/j.cbpa.2011.06.012

Martin, M., Fehsenfeld, S., Sourial, M.M., Weihrauch, D., 2011b. Effects of high environmental ammonia on branchial ammonia excretion rates and tissue Rh-protein mRNA expression levels in seawater acclimated Dungeness crab Metacarcinus magister. Comp. Biochem. Physiol. - A Mol. Integr. Physiol. 160, 267–277. https://doi.org/10.1016/j.cbpa.2011.06.012

Martinelle, K., Häggström, L., 1993. Mechanisms of ammonia and ammonium ion toxicity in animal cells: Transport across cell membranes. J. Biotechnol. 30, 339–350. https://doi.org/10.1016/0168-1656(93)90148-G

Masui, D.C., Furriel, R.P.M., Mantelatto, F.L.M., McNamara, J.C., Leone, F.A., 2003. Gill (Na+,K+)-ATPase from the blue crab Callinectes danae: Modulation of K+-phosphatase activity by potassium and ammonium ions. Comp. Biochem. Physiol. - B Biochem. Mol. Biol. 134, 631–640. https://doi.org/10.1016/S1096-4959(03)00024-1

Matsuo, N., Kawamoto, S., Matsubara, K., Okubo, K., 1997. Cloning of a cDNA encoding a novel sugar transporter expressed in the neonatal mouse hippocampus. Biochem. Biophys. Res. Commun. 238, 126–129. https://doi.org/10.1006/bbrc.1997.7252

McGaw, I.J., 2005. Burying behaviour of two sympatric crab species: Cancer magister and Cancer productus. Sci. Mar. 69, 375–381. https://doi.org/10.3989/scimar.2005.69n3375

Nakada, T., Westhoff, C.M., Kato, A., Hirose, S., 2007. Ammonia secretion from fish gill depends on a set of Rh glycoproteins. FASEB J. 21, 1067–1074. https://doi.org/10.1096/fj.06-6834com

Nash, N., Klymasz-Swartz, A.K., Nash, M.T., Sachs, M., Yoon, G.R., Weihrauch, D., 2022. Impact of heatwaves and environmental ammonia on energy metabolism, nitrogen excretion, and mRNA expression of related genes in the indicator model system Daphnia magna. Aquat. Toxicol. 249, 106225. https://doi.org/10.1016/j.aquatox.2022.106225

Nawata, M., Wood, C.M., O'Donnell, M.J., 2010. Functional characterization of Rhesus glycoproteins from an ammoniotelic teleost, the rainbow trout, using oocyte expression and SIET analysis. J. Exp. Biol. 213, 1049–1059. https://doi.org/10.1242/jeb.038752

Norenberg, M.D., Huo, Z., Neary, J.T., Roig-Cantesano, A., 1997. The glial glutamate transporter in hyperammonemia and hepatic encephalopathy: Relation to energy metabolism and glutamatergic neurotransmission. Glia 21, 124–133. https://doi.org/10.1002/(SICI)1098-1136(199709)21:1<124::AID-GLIA14>3.0.CO;2-U

O'Donnell, M.J., 1997. Mechanisms of Excretion and Ion Transport in Invertebrates. Compr. Physiol. 1207–1289. https://doi.org/10.1002/cphy.cp130217

Obenauer, J.C., Cantley, L.C., Yaffe, M.B., 2003. Scansite 2.0: Proteome-wide prediction of cell signalling interactions using short sequence motifs. Nucleic Acids Res. 31, 3635–3641. https://doi.org/10.1093/nar/gkg584

Omasits, U., Ahrens, C.H., Müller, S., Wollscheid, B., 2014. Protter: Interactive protein feature visualization and integration with experimental proteomic data. Bioinformatics 30, 884–886. https://doi.org/10.1093/bioinformatics/btt607

Parisis, N. (2020, 10 27). Labome- Materials and Methods. Retrieved from Xenopus laevis as a Model System: //dx.doi.org/10.13070/mm.en.2.151

Pawson, T., Scott, J.D., 1997. Signaling through scaffold, anchoring, and adaptor proteins. Science (80-.). 278, 2075–2080. https://doi.org/10.1126/science.278.5346.2075

Pfaffl, M.W., 2004. Quantification strategies in real-time PCR, in: A-Z of Quantitative PCR. pp. 87–112. https://doi.org/10.1029/JA089iA05p02945

Quijada-Rodriguez, A.R., Treberg, J.R., Weihrauch, D., 2015. Mechanism of ammonia excretion in the freshwater leech nephelopsis obscura: Characterization of a primitive Rh protein and effects of high environmental ammonia. Am. J. Physiol. - Regul. Integr. Comp. Physiol. 309, R692–R705. https://doi.org/10.1152/ajpregu.00482.2014

Serrano, L., Henry, R.P., 2008. Differential expression and induction of two carbonic anhydrase isoforms in the gills of the euryhaline green crab, Carcinus maenas, in response to low salinity. Comp. Biochem. Physiol. - Part D Genomics Proteomics 3, 186–193. https://doi.org/10.1016/j.cbd.2008.02.003

Si, L., Pan, L., Wang, H., Zhang, X., 2018. Identification of the role of Rh protein in ammonia excretion of the swimming crab Portunus trituberculatus. J. Exp. Biol. 221. https://doi.org/10.1242/jeb.184655

Spaargaren, D.H., 1990. The effect of total environmental CO2 concentrations on the ion-permeability of shore crabs, Carcinus maenas (L.). Comp. Biochem. Physiol. -- Part A Physiol. 95, 87–91. https://doi.org/10.1016/0300-9629(90)90236-L

Thiel, D., Hugenschutt, M., Meyer, H., Paululat, A., Quijada-Rodriguez, A.R., Purschke, G., Weihrauch, D., 2017. Ammonia excretion in the marine polychaete Eurythoe complanata (Annelida). J. Exp. Biol. 220, 425–436. https://doi.org/10.1242/jeb.145615

Towle, D.W., Mangum, C.P., Johnson, B.A., Mauro, N.A., 1982. The role of the Coxal Gland in Ionic, Osmotic, and pH Regulation in the Horseshoe Crab Limulus polyphemus. Physiol. Biol. Horseshoe Crabs 147–172.

Verdouw, H., Van Echteld, C.J.A., Dekkers, E.M.J., 1978. Ammonia determination based on indophenol formation with sodium salicylate. Water Res. 12, 399–402. https://doi.org/10.1016/0043-1354(78)90107-0

Weihrauch, D., Allen, G.J.P., 2018. Ammonia excretion in aquatic invertebrates: new insights and questions. J. Exp. Biol. 221, 1–11. https://doi.org/10.1242/jeb.178673

Weihrauch, D., Becker, W., Postel, U., Luck-Kopp, S., Siebers, D., 1999. Potential of active excretion of ammonia in three different haline species of crabs. J. Comp. Physiol. - B Biochem. Syst. Environ. Physiol. 169, 25–37. https://doi.org/10.1007/s003600050190

Weihrauch, D., Becker, W., Postel, U., Riestenpatt, S., Siebers, D., 1998. Active excretion of ammonia across the gills of the shore crab Carcinus maenas and its relation to osmoregulatory ion uptake. J. Comp. Physiol. - B Biochem. Syst. Environ. Physiol. 168, 364–376. https://doi.org/10.1007/s003600050156

Weihrauch, D., Morris, S., Towle, D.W., 2004. Ammonia excretion in aquatic and terrestrial crabs. J. Exp. Biol. 207, 4491–4504. https://doi.org/10.1242/jeb.01308

Weihrauch, D., Ziegler, A., Siebers, D., Towle, D.W., 2002. Active ammonia excretion across the gills of the green shore crab Carcinus maenas: Participation of Na+/K+-ATPase, V-type H+-ATPase and functional microtubules. J. Exp. Biol. 205, 2765–2775.

Wright, P.A., 1995. Nitrogen excretion: Three end products, many physiological roles. J. Exp. Biol.

Wright, P.A., Wood, C.M., 2009. A new paradigm for ammonia excretion in aquatic animals: Role of rhesus (RH) glycoproteins. J. Exp. Biol. 212, 2303–2312. https://doi.org/10.1242/jeb.023085

Young-Lai, W.W., Charmantier-Daures, M., Charmantier, G., 1991. Effect of ammonia on survival and osmoregulation in different life stages of the lobster Homarus americanus. Mar. Biol. 110, 293–300. https://doi.org/10.1007/BF01313716

Zhouyao, H., Fehsenfeld, S., Weihrauch, D., Eck, P., 2022. The Human Major Facilitator Superfamily Domain Containing 14A (MFSD14A) Gene Does Not Encode a Glucose Transporter. Adv. Nutr. Food Sci. 2022, 1–13.

Appendices

Supplementary Table 1. Primer sequences used in qPCR in the gill regions of *Limulus polyphemus.* Na^+/K^+-ATPase α-subunit (NKA), V-type H^+-ATPase subunit B (HAT), Rhesus-protein 1 (LpRh-1), Rhesus-protein 2 (LpRh-2), cytoplasmic carbonic anhydrase (CA-2) were used as target genes in qPCR, whereas elongation factor-1α (EF-1α) was used as the housekeeping gene. F= forward primer, R= reverse primer.

Transcript name	Sequence (5'-3')	Amplicon size (bp)	Annealing temperature (°C)
NKA F	CTAGGTGGACTTGGAGAGCG	128	58
NKA R	CCCACCAAACGCATATTACC		
HAT F	CTGAATTCCTGGCCTACCAA	100	58
HAT R	TCACGTGCAGCTGATACCTC		
LpRh-1 F	TGGTTTCATCTCGGTTATGGG	173	58
LpRh-1 R	AGCTGTAACCGTAGTTGTCTTC		
LpRh-2 F	CCCTGTTCAATTGGTTGTGATG	190	58
LpRh-2 R	GGTCTTTAGAGGGATCCTGAAG		
CA-2 F	ACTTACCACCCCTCCCTGTT	191	58
CA-2 R	CCCTATCACCTATCGGCAAA		
LpEF1α F	GGCTACAATCCTGCCACTGT	122	58
LpEF1α R	GTTTGACCCTTGCGTTCAAT		

Supplementary Table 2. GenBank accession numbers for HIAT1 amino acid sequences

Genbank Accession #	Species	Common name	Class	Subclass/Order
NP_001087834.1	*Xenopus laevis Hiat1a*	African clawed frog	Amphibia	Pipidae
NP_001085612.1	*Xenopus laevis Hiat1b*	African clawed frog	Amphibia	Pipidae
XP_018114716.1	*Xenopus laevis Hiat1-like*	African clawed frog	Amphibia	Pipidae
GBM51218.1	*Araneus ventricosus*	Orb-weaving spider	Arachnida	Aranea
KAF8763391.1	*Argiope bruennichi*	Wasp spider	Chelicerata	Arachnida
XP_002433605.3	*Ixodes scapularis*	Deer tick	Chelicerata	Arachnida
XP_013785386.1	*Limulus polyphemus HIAT1β*	American horseshoe crab	Chelicerata	Xiphosura
XP_013778555.1	*Limulus polyphemus HIAT1α*	American horseshoe crab	Chelicerata	Xiphosura
GFT51971.1	*Nephila pilipes*	Golden orb weaver	Chelicerata	Arachnida
XP_015911174.1	*Parasteatoda tepidariorum*	Common house spider	Chelicerata	Arachnida
KAB7505624.1	*Armadillidium nasatum*	Pillbug	Crustacea	Isopoda
QWK64011.1	*Carcinus maenas*	Green crab	Crustacea	Decapoda
XP_042223328.1	*Homarus americanus*	American lobster	Crustacea	Decapoda
XP_018014852.1	*Hyalella azteca*	Mexican freshwater shrimp	Crustacea	Amphipoda
XP_040583787.1	*Lepeophtheirus salmonis*	Salmon louse	Crustacea	Copepoda
TRY78612.1	*Tigriopus californicus*	Tigger pods	Crustacea	Copepoda
CBQ72270.1	*Sporisorium reilianum*		Fungi	
XP_021695504.1	*Aedes aegypti*	Yellowfever Mosquito	Insecta	Diptera
XP_006560033.1	*Apis mellifera*	Honey bee	Insecta	Hymenoptera
NP_647771.1	*Drosophila melaogaster*	Fruit fly	Insecta	Diptera
XP_046821760.1	*Vespa crabro*	European hornet	Insecta	Hymenoptera
XP_021930139.1	*Zootermopsis nevadensis*	Nevada termite	Insecta	Isoptera
NP_149044.2	*Homo sapiens*	Human	Mammalia	Primates
XP_002113942.1	*Trichoplax adhaerens*		Placozoa	
XP_004142991.1	*Cucumis sativus*	Cucumber	Plantae	
AAH56817.1	*Danio rerio HIAT1a*	Zebrafish	Teleostei	Cypriniformes
AAH97075.1	*Danio rerio HIAT1b*	Zebrafish	Teleostei	Cypriniformes
XP_002663499.2	*Danio rerio HIAT1-like*	Zebrafish	Teleostei	Cypriniformes
XP_020335852.1	*Oncorhynchus kisutch*	Coho salmon	Teleostei	Salmoniformes
XP_026143900.1	*Carassius auratus Hiat1a*	Goldfish	Teleostei (FW)	Cyprinidae
XP_026091418.1	*Carassius auratus Hiat1b*	Goldfish	Teleostei (FW)	Cyprinidae
XP_026076322.1	*Carassius auratus Hiat1-like*	Goldfish	Teleostei (FW)	Cyprinidae
XP_014047397.1	*Salmo salar Hiat1a*	Atlantik salmon	Teleostei (SW)	Salmonidae
XP_014071494.1	*Salmo salar Hiat1b*	Atlantik salmon	Teleostei (SW)	Salmonidae
XP_013981624.1	*Salmo salar Hiat1-like*	Atlantik salmon	Teleostei (SW)	Salmonidae